Centrosomal Enrichment and Proteasomal Degradation of SYS-1/β-catenin Requires the Microtubule Motor Dynein

Joshua W. Thompson, Maria F. Valdes Michel, Bryan T. Phillips

Abstract

The *C. elegans* Wnt/β-catenin Asymmetry (WβA) pathway utilizes asymmetric regulation of SYS-1/β-catenin and POP-1/TCF coactivators. This differentially regulates gene expression during cell fate decisions, specifically by asymmetric localization of determinants in mother cells to produce daughters biased towards their appropriate cell fate at birth. Despite the induction of asymmetry, β-catenin localizes symmetrically to mitotic centrosomes in both mammals and *C. elegans*. Due to the mitosis-specific mobility of centrosomal SYS-1 and 'traffic jam' like enrichment of SYS-1 at kinetochore microtubules when SYS-1 centrosomal loading is disrupted, we investigated active trafficking in SYS-1 centrosomal localization. Here, we demonstrate that trafficking by microtubule motor dynein is required to maintain SYS-1 centrosomal enrichment, by dynein RNAi-mediated decreases in SYS-1 centrosomal enrichment and by temperature-sensitive allele of the dynein heavy chain. Conversely, we observe that depletion of microtubules by Nocodazole treatment or RNAi of putative dynein-proteasome adapter ECPS-1 exhibits increased centrosomal enrichment of SYS-1. Moreover, disruptions to SYS-1 or negative regulator microtubule trafficking are sufficient to significantly exacerbate SYS-1 dependent cell fate misspecifications. We propose retrograde microtubule-mediated trafficking enables SYS-1 and negative regulators to enrich at centrosomes, enhancing their interaction and perhaps implicating the centrosome as a mitotic sink for proteins targeted for degradation.

Keywords

Development, Wnt, β-catenin, microtubule, ECM29, dynein, proteasome, trafficking, elegans, asymmetry, cell cycle, robustness

Introduction

During metazoan development, cells must robustly respond to and integrate multiple signaling pathways to appropriately specify and populate tissues. This is of further importance in the developing embryo, where cell division rapidly alternates between S-phase and mitosis while simultaneously specifying tissues and entire germ layers (Pintard and Bowerman 2019). As such, the cell's response to these signals and the subsequent establishment of asymmetry often begins before asymmetric daughter cells are even 'born' via an asymmetric cell division (ACD) (Sunchu and Cabernard 2020; Juanes, 2020; Fuchs and Chen, 2013; Gómez-López, Petrisch et al 2014). Among the signaling pathways utilized in development is Wnt/β-catenin signaling, wherein the binding of Wnt ligands disrupts β-catenin degradation via dismantling an intracellular destruction complex. This effectively stabilizes β-catenin, enabling it to activate target genes with co-activator TCF/LEF (Nusse and Clevers 2017). Wnt/β-catenin signaling is specialized in its ability to regulate both polarity and proliferation – enabling developing organisms to orient and expand tissues simultaneously for appropriate size and morphology (Loh et al 2016). For this reason, Wnt/β-catenin signaling is readily adaptable throughout development to the adult organism.

Wnt/β-catenin is particularly well adapted to the organization of a patterned stem cell niche for proliferative tissue maintenance (Pinto, Clevers et al 2003; Reilein, Kalderon et al 2017). However, this function in adult tissue homeostasis also associates deleterious dysregulation of Wnt/β-catenin signaling with disease states. Throughout transduction of the Wnt signal are proteins vulnerable to oncogenic mutation (Yang, yen 2011; Zhunussova, Djansugurova et al 2019; Liu, Thibodeau et al 2000). However, these often affect their tumorigenicity via dysregulation of the pathway effector β-catenin, which can promote proliferation via over-and mis-expression of targets like Cyclin D1 and cMyc (Niehrs, Acebron 2012; He, Kinzler et al 1998; Shtutman, Ben-Ze'ev et al 1999; Tetsu and McCormick, 1999). Moreover, β-

51 catenin is a bifunctional protein in mammalian systems. That is, it is distributed between the previously
52 described signaling role while also maintaining cell-cell adhesion at adherens junctions (Niehrs, Acebron
53 2012; Reya, Clevers 2005), where it facilitates the interaction between membrane protein E-cadherin
54 and the cytoskeleton. The combination of these roles for β-catenin makes it both an attractive target for
55 studying tumorigenesis, both due to hyperproliferative phenotypes and ease of metastasis. However,
56 the dual functions can also lead to confounding pleiotropic phenotypes after manipulation of β-catenin
57 activity (Reya, Clevers 2005; Tejpar, Alman et al 1999; Geyer, Reis-Filho et al 2011).

58 *C. elegans*, unlike the canonically described Wnt signaling pathway, has distributed the adhesive
59 and signaling roles across its four β-catenins (Sawa, 2012). Here we focus specifically on the *C. elegans*
60 β-catenin SYS-1 for its role as a transcriptional activator in a modified Wnt/β-cat signaling pathway, the
61 Wnt/β-catenin Asymmetry pathway(WβA) (Phillips, Kimble et al 2007). The WβA pathway is a
62 specialized application of the more basic Wnt signaling paradigm, wherein regulation of the co-activator
63 SYS-1 (β-catenin) modulates the activity of transcription factor POP-1 (TCF), during asymmetric cell
64 division (Baldwin and Phillips 2018, Lam and Phillips 2017). That is, dividing mother cells polarize
65 components of the Wnt signaling pathway to a cortical region which will appropriately benefit the
66 daughter cell inheriting that cortex – distributing positive regulators of a Wnt response to the signaled
67 pole of the cell, and negative regulators to the unsignaled pole (Baldwin and Phillips 2014; Baldwin,
68 Phillips et al 2016; Sugioka, Sawa et al 2011). Daughter cells in such a division therefore inherit Wnt
69 signaling components that bias them toward their appropriate cell fate. Contrary to its known role of
70 asymmetrically activating Wnt target genes the key transcriptional effector of this pathway, SYS-1 (and
71 indeed, mammalian β-catenin (Mbom, Barth et al 2014; Vora, Phillips et al 2020)), unexpectedly
72 localizes symmetrically to mother cell mitotic centrosomes (Phillips, Kimble et al 2007; Huang, Lin et al
73 2007; Vora and Phillips 2015).

74 Previous work has demonstrated that mother cell centrosomal localization of SYS-1 limits SYS-1
75 levels in daughter cells in a proteasome dependent manner (Vora and Phillips 2015). Differential
76 localization of the proteasome during the cell cycle (Amsterdam, Baumeister et al 1993), as well as
77 interactor-specific localization of the proteasome for intracellular structuring (Baldin, Coux et al 2008),
78 suggest that proteasome regulation, localization, and activity are interdependent. Proteasomal subunits
79 have, for example, been shown to co-sediment with centrosomal proteins and perinuclear inclusions
80 indicative of centrosomal localization (Wigley, Thomas et al 1999; Wojcik, DeMartino 2003). Similarly,
81 centrosomal localization is required for mitotic clearance of SYS-1, such that uncoupling SYS-1 from
82 centrosomes results in daughter cells exhibiting approximately 40% more SYS-1 protein. Moreover, SYS-
83 1 turnover by FRAP mobile fraction at centrosomes is dependent on RPT-4 proteasomal activity (Vora
84 and Phillips 2015). Perhaps, then, the centrosome is a region where SYS-1 – proteasome interactions are
85 concentrated to regulate its retention and effect on cell fate.

86 The directionality and temporal specificity of this mitotic enrichment and degradation implied
87 that a more active localization mechanism might be at work, compared to a more passive captured
88 diffusion mechanism. This is most directly demonstrated in that the cell maintains a proteasome-
89 dependent, 100% mobile population of centrosomal SYS-1, which is recycled within 120 seconds (Vora
90 and Phillips 2015). Cells appear to maintain this robust and dynamic localization of SYS-1 specifically on
91 the mitotic centrosome, with the interphase centrosome undetectable via SYS-1 fluorescence (Vora and
92 Phillips 2015). However, the mechanism of such temporally specific SYS-1 centrosomal localization is
93 unknown. Several observations indicate that cells utilize the microtubule cytoskeletal network for rapid
94 and directional regulation of specific cargo to precise locales, including: that dynein conditionally traffics
95 transcription factors due to neuronal injury or signaling status, (Ben-Yaakov, Fainzilber et al 2012;
96 Mikenberg, Kaltschmidt et al 2007) and that dynein more generally can enrich endocytic recycling
97 components around the Microtubule Organizing Center (MTOC) (Horgan, Mccaffrey et al 2011) or be

98 sufficient to prevent pathogenic accumulation of RNA binding proteins (Deshiumaru, Tsuboi et al 2021).
99 Therefore, we hypothesized that the role of the mitotic centrosome as an MTOC could facilitate the
100 rapid transport of SYS-1 to the pericentriolar material specifically in dividing cells.

101 The rapid and cell cycle phase-specific enrichment of SYS-1 at the centrosome suggests that it
102 may also depend on active transport. Further, accumulation at a highly active MTOC like the mitotic
103 centrosome is most likely accomplished by the microtubule minus end-directed dynein motor complex
104 (Vora and Phillips 2015; Priyanga, Bhaka-Guha et al 2021). The dynein motor is a multi-subunit complex
105 composed of a pair of ATP-ase, microtubule-binding heavy chains responsible for the force-generating
106 steps of the motor, and a variable complement of smaller light, intermediate, and accessory chains that
107 alter the cargo binding or processivity of the motor (Reck-Peterson, Carter et al 2018; Jha and Surrey
108 2015). The dynein motor is multifunctional - it provides pulling forces, positions organelles, and can
109 mediate rapid and conditional movement of proteins and RNAs (Carminati and Stearns 1997; Woźniak,
110 Allan et al 2009; Harada, Hirokawa et al 1998; Hanz, Fainzilber et al 2003; Bullock and Ish-Horowicz
111 2001). For example, injured rat axons have demonstrated a dynein intermediate chain-dependent
112 nuclear localization and coimmunoprecipitation of the transcription factor STAT3, in order to
113 appropriately adopt an injury-dependent transcriptional response (Ben-Yaakov, Fainzilber et al 2012).
114 Dynein specifically is the motor complex most often directed towards the MTOC and is known to be
115 active during mitosis (Jha and Surrey 2015). Therefore, we investigated dynein-dependent trafficking as
116 an ideal mechanism for SYS-1 localization to the MTOC mitotic centrosomes.

117 Here we demonstrate that microtubules and minus-end microtubule-mediated trafficking are
118 required for the centrosomal recruitment of both SYS-1 and the negative regulators responsible for its
119 regulation there. We evaluate the extent to which SYS-1 utilizes dynein-mediated trafficking to
120 accumulate at centrosomes (Fig. 1A). Using both long- and short-term disruptions to dynein and
121 microtubule-mediated trafficking to evaluate SYS-1 localization and SYS-1-dependent cellular activity up

122 to and including cell fate changes, we demonstrate that SYS-1 and its negative regulators both require
123 microtubule-mediated trafficking for appropriate regulation of SYS-1 (Fig. 1B-D). Together, these data
124 characterize a system for enhancing the robustness of the WβA signaling pathway by maintaining
125 consistent interaction of SYS-1 with negative regulators at the mitotic centrosome.

126 **Results**

127 **SYS-1 Overexpression and Centrosomal Uncoupling Results in SYS-1 Accumulation at Regions of**
128 **Dynein Enrichment**

129 To test the role of microtubule-mediated trafficking in SYS-1 centrosomal localization, we
130 investigated what trafficking mechanisms are necessary for SYS-1 regulation. We compared
131 fluorescently tagged SYS-1 protein localization to that of MT trafficking components. Of most interest
132 was the cytoplasmic dynein motor complex, since its components have been shown to localize to mitotic
133 centrosomes, kinetochore microtubules, and cortically across species (Schmidt, Van den Heuvel et al
134 2017; Tame, Medema et al 2014). This corresponded to GFP::SYS-1 , which localizes to these same
135 cortical and microtubule dense regions. Moreover, this localization was more common upon
136 centrosomal uncoupling by RNAi depletion of the spindle assembly and scaffolding protein RSA-2(Fig
137 2A). While GFP::SYS-1 has been observed at mitotic centrosomes throughout the organism,
138 accumulation at these cortical and kinetochore 'secondary' sites is uncommon (accumulation at either
139 or both of these sites occurring in 34.5% of embryos) in untreated organisms but the frequency of this
140 accumulation approximately doubles, to 69.1%, with *rsa-2(*RNAi) (Fig2A). This finding is consistent with
141 'traffic jams' observed in microtubule mediated trafficking, often aggravated by decreasing microtubule-
142 off rate (Leduc, Howard et al 2012).

143 Untreated, GFP::SYS-1 expression, driven by the strong germline/embryonic PIE-1 promoter, is
144 likely expressed at higher-than-wildtype levels. This increase, in addition to potentially rate limiting

145 protein interactions required for RSA-2 mediated centrosomal capture, may bottleneck SYS-1 at the
146 point of centrosomal capture. The centrosomal uncoupling seen in *rsa-2*(RNAi) has also been shown to
147 increase SYS-1 protein in resulting daughter cells, in addition to the previously described loss of
148 centrosomal enrichment (Vora and Phillips 2015). This suggests that increases in intracellular SYS-1,
149 along with a lower SYS-1/dynein 'off' rate from microtubules by the centrosomal 'sink', are sufficient to
150 overwhelm the centrosomal degradation mechanisms of SYS-1 and crowd centrosome-bound motor
151 complexes in microtubule motor 'traffic jams'. That is, by decreasing SYS-1 microtubule on-rate due to
152 disruptions in motor complex formation, or decreasing its microtubule off-rate by disrupting
153 centrosomal capture by RSA-2, we can observe GFP::SYS-accumulation throughout the process of
154 trafficking - at regions of dynein loading and unloading, respectively, as well as regions of high
155 microtubule occupancyas the off-rate 'traffic jam' worsens (Leduc, Howard et al 2012). The
156 enhancement of SYS-1 kinetochore and cortex localization seen in *rsa-2(RNAi),* with the coinciding
157 centrosomal uncoupling, is therefore consistent with *rsa-2(RNAi)* reducing the SYS-1 microtubule-off
158 rate and exhibiting more frequent, or worse, traffic jams.

159 **Knockdown of Dynein Complex Subunits Reduces SYS-1 Centrosomal Localization**

160 Given the observation that SYS-1 localizes to these sites important for trafficking via the
161 retrograde dynein motor, we investigated a functional role for the dynein complex in SYS-1 localization.
162 We began by performing an RNAi screen against various components of the dynein motor complex and
163 associated proteins, eventually expanding outward to additional motors and microtubule-affecting
164 proteins (Fig S1). Specifically, by RNAi depletion of these microtubule trafficking proteins, we assayed
165 the centrosomal steady state of GFP::SYS-1. We expected depletion of transport proteins that play a role
166 in SYS-1 centrosomal transport to be defective in the maintenance of SYS-1 centrosomal enrichment
167 when SYS-1 centrosomal clearance was otherwise unaffected. In order to evaluate the centrosome-
168 specific enrichment of SYS-1, we considered two ways of measuring fluorescently-tagged SYS-1 steady

169 state levels: 1) the centrosomal enrichment index (CEI)(similar to that described in Gao, Smith et al
170 2017), the centrosomal fluorescence intensity adjusted by subtraction of the background cytoplasmic
171 fluorescent intensity of the surrounding cell, to control for backgrounds that may pleiotropically
172 influence SYS-1 expression, and 2) the SYS-1 CEI evaluated as a ratio to the same enrichment factor of
173 representative PCM factor γ-tubulin (Tubulin Enrichment Index, or TEI) , to avoid false positives via
174 defects in PCM maturation (CEI/TEI) (Fig 2B-B''). We then compared these centrosomal enrichment
175 metrics to those seen in established *rsa-2(*RNAi) centrosomal uncoupling.

176 As expected, depletion of several dynein subunit knockdowns presented pleiotropic and
177 deleterious effects, including oogenesis and early patterning defects which precluded our SYS-1
178 localization assay. We therefore treated organisms with partial RNAi knockdowns by commencing RNAi
179 feeding 12-24 hours before imaging as necessary, based on the phenotypic severity. While no
180 treatment disrupted SYS-1 centrosomal steady state sufficiently to lose any apparent SYS-1 centrosomal
181 accumulation as seen in *rsa-2*(RNAi), we did observe several statistically significant decreases in
182 centrosomal SYS-1 enrichment (Fig S1,2C – C'). Furthermore, while the total population of some
183 treatments displayed only an intermediate mean loss of SYS-1 enrichment, the distribution of SYS-1 CEI
184 values observed in dynein subunit knockdowns extends from wild-type to an *rsa-2(RNAi)*-like disruption
185 (e.g. Fig. S2). These decreases, and notably lower minimum, in SYS-1 CEI or CEI/TEI are masked
186 somewhat in the population average by this broad range in phenotype and/or RNAi penetrance (Fig 2C-
187 C', Fig S2). Most notably, *dlc-1(RNAi)* and *dylt-1(RNAi)* each exhibit a significant γ-tubulin-independent
188 reduction in centrosomal SYS-1 localization. This centrosomal uncoupling was specifically more visible in
189 a transgene driven by the endogenous SYS-1 promoter, as compared to SYS-1 driven by a stronger and
190 likely overexpressing germline/early embryo promoter (Fid 2C-C').

191 These data suggest that dynein does have a role in the localization of SYS-1 to centrosomes, but
192 redundancy between components of the dynein motor or between the dynein motor and other
193 processes may limit the effect any one subunit has on SYS-1 localization. Alternately, while mutants are
194 often severely deleterious, variability of RNAi efficacy may have resulted in incomplete depletion of SYS-
195 1 relevant dynein subunits. Similarly, the pleiotropic effects of dynein depletion may also have
196 superseded effects on SYS-1 localization, leading to the evaluation of only partial knockdowns. In order
197 to address these issues, we investigated the role of the dynein motor in SYS-1 localization at a more
198 precise temporal resolution via conditional dynein disruption.

199 **Temporally Restricted Dynein Loss of Function Reveals Dynein Requirement for Centrosomal Steady**
200 **State SYS-1 Accumulation.**

201 While our screen showed that dynein knockdown results in significant reduction of centrosomal
202 SYS-1, with rare individuals exhibiting *rsa-2(RNAi)*-like loss of centrosomal SYS-1 accumulation, we were
203 unable to completely recreate a population exhibiting consistently severe disruption to SYS-1 CEI. To
204 distinguish the variety in effect on SYS-1 localization effects between functional redundancies limiting
205 the effects of dynein depletion and the confounding deleterious effects described above, we utilized a
206 temperature sensitive allele of the cytoplasmic dynein heavy chain, *dhc-1(or195ts),* to conditionally
207 inactivate this cytoplasmic dynein heavy chain. This allele, identified in the Bowerman lab, introduces a
208 lesion to the microtubule binding stalk of DHC-1. This lesion renders the motor slightly hypomorphic,
209 even at the permissive 15°C (with only 91% of embryos hatching), but still sufficiently functional to form
210 bipolar spindles and generate pulling force throughout the cell, with homozygotes remaining viable and
211 fertile at permissive temperatures (Hamill, Bowerman et al 2002). However, after upshifting to 26°C,
212 *dhc-1(ts)* mutants undergo complete mitotic spindle collapse as little as 30 seconds, suggesting that
213 DHC-1 motor function has been nearly completely ablated (O'rourke, Bowerman et al. 2007). Therefore,

214 we expected that replicating this treatment in a strain containing both *dhc-1(ts)* and fluorescently
215 tagged SYS-1 would allow us to examine a more penetrant dynein knockdown while overcoming both
216 potential redundancy between dynein accessory chains in the trafficking of SYS-1 and pleiotropic effects
217 precluding the observation of mitotic centrosomal SYS-1 (Fig. 3A). As described above, we compared the
218 CEI of the endogenous promoter-driven VENUS::SYS-1 driven by the endogenous SYS-1 promoter to that
219 of mCherry::γ-Tubulin (TEI) to control for changes in centrosome size and maturation that may
220 otherwise confound changes specific to SYS-1 centrosomal steady state. Consistent with the published
221 hypomorphic nature of the allele at the permissive temperature (O'rourke, Bowerman et al 2007),
222 imaging *dhc-1(ts)* embryos, shows notable decrease in the SYS-1 CEI of embryos kept at the permissive
223 temperature (Fig 3 B-D). Following 30-45 seconds of temperature upshift, this hypomorphic phenotype
224 is enhanced to severely reduce SYS-1 centrosomal enrichment (Fig 3B-C). While there was a decrease in
225 centrosome size, presumably due to roles for dynein in centrosome maturation (Priyanga, Bhakta-Guha
226 et al 2021), the CEI/TEI metric accounted for this. We observed a CEI/TEI decrease corresponding to
227 decreased centrosomal SYS-1 accumulation, proportionally greater than the reduction in γ-tubulin (Fig
228 3D'). Combined with the individual dynein subunit knockdown, the more penetrant phenotype of *dhc-*
229 *1(ts)* mutants indicates that SYS-1 requires the dynein microtubule motor complex to localize
230 appropriately to centrosomes. Additionally, it seems likely that redundancy of peripheral motor
231 components or incomplete knockdown is responsible for the variability within individual subunit
232 depletions seen above (fig 2C-C').

233 **MT depolymerization experiments reveal that SYS-1 centrosomal dynamics are affected both**
234 **positively and negatively by Microtubule-Mediated trafficking**

235 To determine the extent to which microtubule-based trafficking in general is responsible for SYS-
236 1 centrosomal localization, we treated gravid adults and their embryos with >100 μM Nocodazole, a

237 microtubule-destabilizing agent. This dose, while sufficient for a rapid acute response in adult
238 organisms, caused no effect on fertilized embryos due to their eggshell and prevented the production of
239 additional embryos via germline arrest (data not shown). We therefore turned to a lower dose, longer-
240 term Nocodazole treatment: 12 hours at 25µg/mL (83 µM). This maternal Nocodazole dosing allowed us
241 to obtain embryos with distinctly limited microtubule networks (Fig 4A). Surprisingly, centrosomal and
242 cytoplasmic SYS-1 both increased after Nocodazole treatment (Fig 4B, C). This SYS-1 CEI increase is
243 similar to the phenotype observed in RPT-4 depletion, which decreases proteasome function (Vora and
244 Phillips, 2015), and is consistent with a model wherein negative regulators also require trafficking. In this
245 case, we expect nocodazole induced changes in SYS-1 localization to diverge from those seen in dynein
246 knockdowns by the extent of centrosomal enrichment, but converge on excessive inheritance of
247 GFP::SYS-1 (Fig 1D).

248 The dichotomy of centrosomal SYS-1 depletion or enrichment across dynein or microtubule
249 disruption also provided us an opportunity to evaluate the most basal status of SYS-1 at centrosomes.
250 Moreover, while both temperature upshift for *dhc-1(ts)* and Nocodazole treatments significantly affect
251 SYS-1 centrosomal localization, neither treatment appears to completely disrupt microtubule mediated
252 trafficking. Nocodazole-treated embryos still exhibit some kinetochore microtubules (Fig. 4A) but can
253 tolerate this treatment for some time. Conversely, *dhc-1(ts)* embryos demonstrate such severe loss of
254 dynein function at the restrictive temperature that short-term temperature upshifts are required to
255 establish spindles and maintain viability, suggesting some portion of centrosomal trafficking during
256 mitosis still occurs. For this reason, we suspected the combination of these treatments could most
257 severely limit dynein trafficking. A nocodazole-treated, *dhc-1(ts)*-containing organism at the restrictive
258 temperature will likely exhibit the most severely affected dynein trafficking and thus most severely
259 disrupted regulation of SYS-1 on the mitotic centrosome.

260 In fact, studying the combination of these challenges to microtubule-mediated trafficking
261 allowed us to examine several facets of SYS-1 localization. Due to the difference in response to
262 nocodazole based on the promoter driving fluorescently-tagged SYS-1 (Fig 4B, D), we were able to utilize
263 their apparent difference in SYS-1 expression to slightly sensitize organisms to SYS-1/negative regulator
264 defects. In contrast to the GFP::SYS-1 driven by a promoter for ubiquitous early embryonic PIE-1,
265 organisms with YFP::SYS-1 driven by the SYS-1 promoter exhibit only a slight, non-significant,
266 nocodazole-mediated increase in CEI/TEI (Fig. 4D, 1st and 2nd columns). This indicates that the mild
267 overexpression seen in PIE-1 promoter-driven SYS-1 may be sufficient to stress SYS-1 clearance
268 mechanisms, allowing it to more readily overwhelm them in nocodazole treatment. Meanwhile,
269 endogenously driven SYS-1 may be maintained at levels more manageable by the centrosomal clearance
270 mechanism, resulting in a lesser or variable CEI/TEI increase. Importantly, endogenously driven SYS-1 is
271 sufficient to overwhelm centrosomal clearance mechanisms when the hypomorphic *dhc-1(ts)* at
272 permissive temperature is treated with nocodazole, resulting in the same significant increase seen with
273 GFP::SYS-1 (Fig. 4D 3rd and 4th columns, Fig. 4C). However, this increase is no longer observed when the
274 *dhc-1(ts)* organisms are upshifted to the restrictive temperature, indicating that the increasing SYS-1
275 centrosomal enrichment seen in Nocodazole treated embryos still requires some amount of dynein
276 trafficking. These observations describe a centrosomal relationship wherein treatments limiting the
277 coverage of microtubule-mediated dynein trafficking (i.e. nocodazole treatment) increase centrosomal
278 SYS-1 due to relatively inefficient or rare trafficking events for SYS-1 negative regulators, while transient
279 severe disruptions to dynein trafficking processivity (dynein subunit RNAi depletion, *dhc-1(ts)*
280 temperature upshift, upshift + nocodazole) reveal that SYS-1 centrosomal enrichment requires continual
281 replenishment via a functional microtubule motor.

282 If microtubule-mediated trafficking has a potential role for proteasome or other SYS-1 negative
283 regulator centrosomal enrichment, concurrent with SYS-1 localization, we expect approximately similar

284 localization changes as we would for SYS-1. Therefore, we decided to test the idea that proteasomal
285 trafficking to, and enrichment at, the centrosome was also perturbed in nocodazole-affected
286 microtubule networks. We first attempted to localize the proteasome. While the centrosome has been
287 demonstrated to exhibit proteolytic activity (Vora and Phillips 2015; Vora and Phillips 2016; Hames, Fry
288 et al 2005; Peel, O'Connell et al 2012; Wigley, Thomas et al 1999; Fabunmi, DeMartino et al 2000),
289 existing immunohistochemical reagents for mammalian proteasome subunits did not display any distinct
290 localization pattern. An mCherry tag on proteasome subunit RPT-1 did demonstrate a kinetochore
291 microtubule enrichment like that of both DHC-1 and SYS-1 but appeared absent from centrosomes. This
292 may be due to a relatively low RPT-1 copy number per proteasome, or correspondingly low proteasome
293 number per centrosome, limiting its relative enrichment there. Alternatively, fluorescently tagged
294 proteins have shown evidence of degradation of the tag at a site of active proteolysis, particularly if such
295 a tag limits proteasome activity (Huang, Lobel et al 2014). To circumvent this issue, we assayed for
296 centrosomal proteasome activity indirectly by functionally testing an additional target of the
297 centrosomal proteasome, the centriole duplicating kinase ZYG-1 (O'Connell, White et al 2001; Peel,
298 O'Connell et al 2012). In addition, we assayed the centrosomal role of ECPS-1, homolog of mammalian
299 ECM29 and an adaptor protein proposed to enhance proteolytic activity of proteasomes via its function
300 as an adapter between the dynein motor complex and the proteasome (Gorbea, Rechsteiner et al 2010).

301 Knockdown of ECM29 homolog ECPS-1 (formerly d2045.2) resulted in embryos that displayed an
302 average 33.4% increase in centrosomal GFP::SYS-1 centrosomal enrichment, similar to both Nocodazole-
303 treated and *rpt-4(*RNAi) embryos (Fig. 5A, 4 A-C). Given the role of ECPS-1/ECM29 in proteasomal
304 trafficking on MTs rather than direct protein degradation, these data suggest that both SYS-1 and its
305 negative regulator, the proteasome, are trafficked to the centrosome during mitosis. Therefore, the
306 overall increase in SYS-1 CEI seen in *ecps-1*(RNAi) embryos is likely an adjustment of the centrosomal
307 steady state, limiting the trafficking of SYS-1 negative regulators without affecting that of SYS-1. While

308 fluorescently-tagged SYS-1 exhibits widespread localization and expression, allowing for its capture and
309 transport on even a limited microtubule network, the several megadalton proteasome may be
310 dependent on extensive active trafficking. This necessity may be fostered due to both the size and
311 stoichiometry required of the proteasome complex. Indeed, electron micrographs of ECM29, and its
312 interactions with the proteasome, demonstrate that the interaction between ECM29 and the
313 proteasome is at the level of the core 20S proteasome (Leggett, Finley et al 2002). Because of this,
314 longer term microtubule disruption like that of our Nocodazole treatment may prevent the
315 enhancement of centrosomal SYS-1-proteasome interactions while not necessarily preventing SYS-1
316 degradation. That is, the SYS-1 – proteasome interaction is less efficient when not centrosomally
317 concentrated, and prevention of this co-localization should result in increased SYS-1 levels at the
318 centrosome and throughout the cell. To test the activity of the centrosomal proteasome after ECPS-1
319 RNAi treatment, we assayed an additional centrosomal proteasome target – a regulatory kinase of
320 centrosomal duplication called ZYG-1 (Peel, O'Connell et al 2012). Utilizing a fluorescently tagged ZYG-1
321 fragment demonstrated to mirror the localization of the endogenous protein (Peters, O'Connell et al
322 2010), we demonstrated 20% and 27% increased accumulation of ZYG-1 in both proteasome knockdown
323 *rpt-4(RNAi)* and *ecps-1(*RNAi) treatments, respectively, supporting the hypothesis that these shared
324 phenotypes are both proteasome-mediated clearance defects (Fig 5C).

325 Since SYS-1 centrosomal recruitment and regulation of subsequent inheritance depend on rapid
326 degradation via the centrosomal proteasome (Vora and Phillips 2015), we assayed the accumulating
327 centrosomal SYS-1 in *ecps-1(RNAi)* for changes to its steady state dynamics by FRAP. This allowed us to
328 distinguish between increased centrosomal accumulation due to an increased recruitable pool of
329 cytoplasmic SYS-1 when ECPS-1 is depleted as compared to a change in centrosomal steady state due to
330 specific changes to the proteasomal throughput in this locale. Comparison of GFP::SYS-1 recovery after
331 photobleach demonstrates that depletion of ECPS exhibits an intermediate phenotype between

332 proteasome depletion via *rpt-4(RNAi)* and controls (5G-G"). While the initial rate of *ecps-1(RNAi)*
333 GFP::SYS-1 recovery was similar to wild type organisms, the late recovery phase of *ecps-1(RNAi)*
334 organisms showed an early SYS-1 recovery plateau, evidence of a significantly reduced mobile fraction
335 intermediate to wild type and that of proteasome depleted *rpt-4(RNAI)* organisms (Fig 5E,G). This
336 suggests that SYS-1 recovers at an approximately wild type rate in *ecps-1(RNAi)* organisms, but remains
337 approximately as immobile as proteasome-depleted organisms. Therefore, ECPS-1 depleted organisms
338 appear to degrade SYS-1 incompletely, as observed in the RPT-4 proteasome depletion, but with
339 sufficient protein turnover to enable wild type recruitment of newly trafficked SYS-1.

340 This is in contrast to the dynamics observed in other centrosomal proteins. GFP::ZYG-1c exhibits
341 slightly different centrosomal localization dynamics during mitosis from SYS-1, peaking in centrosomal
342 representation mid-anaphase (Peel, O'Connell et al 2012). This suggested that GFP::ZYG-1c is
343 proteasomally degraded, but is most dynamic during early mitosis, maintaining a consistent centrosomal
344 enrichment in anaphase even in *rpt-4(RNAi)* organisms (Peel, O'Connell et al 2012). SYS-1, conversely,
345 exhibits strong centrosomal SYS-1 localization through anaphase and only begins to show decreasing
346 centrosomal levels during telophase (Vora and Phillips 2015). This apparent difference in dynamics is
347 made evident by comparing the recovery after photobleach of GFP::SYS-1 and GFP::ZYG-1c (Fig. 5E-F),
348 wherein both SYS-1 and ZYG-1c become less mobile upon *rpt-4(RNAi)* proteasome depletion but only
349 SYS-1 increases in immobile fraction upon ECPS-1 depletion. This suggests that proteasome depletion
350 by *rpt-4(RNAi)* leads to decreased proteolytic activity that overwhelms and stabilizes the centrosomal
351 proteome, including SYS-1, by preventing turnover. Meanwhile, ECPS-1 depleted organisms may be
352 unaffected in protein clearance per proteasome, but the delayed or partial localization of the
353 centrosomal proteasome could result in hierarchical stabilization of a spatially or temporally inaccessible
354 fraction consisting of highly expressed and continually trafficked proteins, like SYS-1.

355 **Dynein Trafficking is Required for Restriction of Wnt-Signaled Cell Fates**

356 Having established a two-fold role for SYS-1 regulation in microtubule-mediated trafficking, we
357 investigated the role microtubule trafficking played in regulating SYS-1 dependent cell fate decisions.
358 Since the SYS-1 centrosomal localization pattern has been seen across all examined SYS-1-expressing
359 tissues (Phillips, Kimble et al 2007; Huang, Lin et al 2007; Baldwin and Phillips 2018; Lam and Phillips
360 2017), we investigated cell fate changes in embryonic and larval tissues across one embryonic and two
361 larval SYS-1 dependent cell fate decisions. These included the transcriptional reporter of the WβA target
362 gene, *end-1,* in the establishment of SYS-1 dependent endoderm, and an anatomical marker for larval
363 specification of the stem cell-like cells of the hypodermal seam and the germline stem cell niche. First, to
364 directly assay the effect of centrosomal dysregulation of transcriptional activator SYS-1, we investigated
365 the nuclear enrichment of GFP::SYS-1 after the Wnt-regulated EMS division (Bei, Mello et al 2002). In
366 this division, SYS-1 is enriched in the posterior E nucleus, but not that of the anterior MS (Fig. 6A-B).
367 Analyzing nuclear enrichment of GFP-tagged SYS-1, we were able to observe increased nuclear GFP
368 signal in both the E and MS daughters in analyzed trafficking mutants (Fig 6C). Interestingly, daughters
369 affected by both *ecps-1*(RNAi) and *dlc-1*(RNAi) exhibit significant enhancement of nuclear enrichment in
370 each of the two daughter cells (fig 6C), suggesting that these treatments act negatively on SYS-1, despite
371 opposing effect on SYS-1 centrosomal enrichment. Following this loss of negative centrosomal
372 regulation, these data suggest that daughter cell SYS-1 inheritance is increasing and thus affecting the
373 bias of this asymmetric division, increasing the likelihood of unsignaled daughter cells adopting the
374 signaled cell fate.

375 Having established an increase in nuclear GFP::SYS-1 in dynein subunit depletion, even in cells
376 not signaled to maintain activating SYS-1, we turned to the effect of this SYS-1 expression on target gene
377 activation. Specifically, we used the endogenous promoter of WβA target gene *end-1* to drive GFP-

378 tagged Histone 2B in order to evaluate the activity of SYS-1 immediate downstream targets as the
379 signaled E cell established the endoderm tissue expansion from 2 to 4 to 8 cells (E+1, 2, or 3 divisions,
380 respectively). Normally, this strain exhibits additional expression of the *end-1* promoter in <10% of
381 embryos, a frequency which decreases further when SYS-1 is depleted via RNAi (Fig. 6D).. In our
382 embryos depleted of dynein subunits and RSA-2 by RNAi, however, we observed a different pattern. In
383 these embryos, misregulation via dynein depletion appeared to instead increasingly overwhelm SYS-1
384 negative regulation in successive divisions, such that each generation after this SYS-1 dependent
385 specification increasingly expresses this endodermal reporter ectopically outside of the EMS lineage (Fig
386 6D). For instance, in *dhc-1(RNAi)* we observe only 3% of embryos mis-expressing one cell division after
387 the specification of the E cell type (E+1), which increases to 25% by the next division (E+2), and over 83%
388 three divisions after specification (E+3).

389 We also investigated larval ACDs to determine the effect this extra transcriptionally active SYS-1
390 has on organismal development. We examined the seam cells (SCs) and distal tip cells (DTCs) due to
391 their sensitivity to SYS-1 dependent gene activation (Baldwin, Phillips et al 2016; Baldwin and Phillips
392 2018; Lam and Phillips 2017; Mila, Putzke et al 2015). In wild-type animals, DTC lineages undergo
393 asymmetric cell division during L1 to give rise to two DTCs, while *sys-1* mutants and organisms
394 overexpressing SYS-1 show loss and gain of DTCs, respectively, due to symmetric cell division (fig 7A)
395 (Miskowski, Kimble et al 2001; Siegfried, Kimble et al 2004; Kidd, Kimble et al 2005; Chesney, Kimble et
396 al 2009). To further sensitize these cells for changes in SYS-1 dependent cell fate changes, we examined
397 strains containing additional, transgenic SYS-1 driven by the heat shock promoter. In organisms that are
398 not subjected to heat shock, dynein depletion only rarely induced development of more than the
399 endogenous 2 distal tip or 16 seam cells (Fig 7B, 8B). In heat shocked organisms, excess SYS-1 protein
400 can overwhelm canonical SYS-1 regulation to develop as many as 6 DTCs (fig 7D). While heat shock-
401 induced overexpression is sufficient to cause a notable shift towards the signaled cell fate, dynein

402 subunit depletion was able to significantly enhance this (Fig 7C). In the DTC, depletion of DHC-1 or ECPS-
403 1 was sufficient to induce rare but wild-type-unobserved additional distal tip cells (0.3% of organisms for
404 these 2 treatments, N= 394, 363, respectively)). Adding heat shock-overexpressed SYS-1 enhanced the
405 penetrance of ectopic DTCs, with DHC-1 and ECPS-1 depletion resulting in populations where 11.9% and
406 6.8% of organisms, respectively, develop more than 2 DTCs. Depletion of RSA-2, uncoupling SYS-1 from
407 centrosomes, and depletion of a dynein light chain, DYLT-1, further enhanced these misspecifications,
408 increasing the proportion of the population with ectopic DTCs from 26.6% in wild type to 33.6% or 51%
409 after RNAi depletion, respectively (Fig. 7).

410 The SC lineage also undergoes several WBA-dependent ACDs throughout larval development (fig
411 8A). Similarly, in the SC tissue, depletion of dynein light chains alone is sufficient to increase the
412 frequency of ectopic SCs from 3.3% of larvae with ectopics SCs in control RNAi conditions to 11.7% or
413 10% of organisms as seen in DYLT-1 and DLC-1 depletions, respectively (Fig 8B). These misspecifications
414 are further exacerbated by SYS-1 overexpression, wherein more than 60% of the *dylt-1(RNAi)* organisms
415 have greater than wild type seam cell numbers, developing as many as 21 SCs, (Fig. 8C). These
416 observations collectively support SYS-1 centrosomal enrichment by dynein as a mechanism to reinforce
417 SYS-1 function in specifying SYS-1-dependent cell fate decisions. Therefore, compromising this system by
418 dynein depletion is rarely sufficient to induce misspecifications in otherwise wildtype animals, but
419 notably enhances the effects of ectopic SYS-1 accumulation, indicating the robustness of WβA-regulated
420 cell fate decisions after ACD requires SYS-1 negative regulation via dynein-mediated MT transport.

421 **Discussion**

422 Precise control of cell fate determinants is critical for normal development and homeostasis,
423 particularly in the rapidly dividing cells of the early embryo. This regulation includes the distribution and
424 inheritance of these determinants by daughter cells. Here we demonstrate that centrosomal negative

425 regulation of *C. elegans* β-catenin SYS-1 is enhanced during asymmetric division by trafficking to
426 centrosomes by the microtubule motor dynein. Depletion of individual subunits of the dynein motor
427 and associated proteins is sufficient to reduce the centrosomal SYS-1 steady state, and temporally
428 specific ablation of dynein function by *dhc-1(ts)* was sufficient to nearly completely and
429 disproportionately remove observable SYS-1 from centrosomes. However, some methods of disrupting
430 dynein/microtubule trafficking result in an unexpected increase in centrosomal accumulation of SYS-1
431 protein. These increases, caused by microtubule disruption via Nocodazole and depletion of SYS-1
432 negative regulator adapter ECPS-1, were accompanied by SYS-1 CEI steady state adjustments that
433 phenocopy centrosomal enrichment seen in disruption of proteasome activity, and further maintain a
434 SYS-1 immobile fraction like that seen in proteasome disruption experiments. We therefore propose a
435 model wherein both SYS-1 and its negative regulators, including the proteasome, are dependent on
436 microtubule-mediated trafficking to centrosomes by the dynein complex in order to appropriately
437 reinforce SYS-1 asymmetric cell divisions (Fig 9). In this model, SYS-1 requires continual trafficking by
438 microtubule motors to maintain its observable steady state, suggesting highly efficient interactions with
439 the dynein molecule while exhibiting vulnerability to subtle disruptions to dynein trafficking. Conversely,
440 the enzymatic substrate processing of the proteasome requires fewer proteasome complexes to be
441 trafficked, making it less vulnerable to short term disruptions to trafficking but requiring a robust
442 microtubule network to secure these relatively fewer events.

443 While this system of centrosomal localization and clearance of SYS-1 does not appear necessary
444 for most WβA differentiation events, disruptions to this system increasingly limit its ability to tolerate
445 perturbations. This suggests that SYS-1 centrosomal localization thereby generates robustness in SYS-1
446 dependent cell fate decisions (Fig 6-8). This set of parallel and synergistic trafficking mechanisms
447 accounts for the similar excess SYS-1 found in affected daughter cells of mothers with both increased
448 and decreased centrosomal recruitment of SYS-1. That is, disruption of either SYS-1 localization

449 (inefficient trafficking to the site of regulation) or disruption of proteasomal localization (SYS-1 is
450 trafficked and accumulates, but centrosomal degradation is ineffective) both result in increased SYS-1
451 protein in daughter cells, consistent with excessive inheritance.

452 Why does no single dynein disruption treatment fully recapitulate the *rsa-2(RNAi)* phenotype?
453 While we do see individuals within several dynein knockdown treatments with nearly *rsa-2(RNAi)*-like
454 SYS-1 centrosomal uncoupling, these populations also include organisms with roughly wild type
455 centrosomal SYS-1, unlike those in *rsa-2*(RNAi). However, given the severely deleterious nature of
456 dynein subunit loss-of-functions (Sönnichsen, Neumann et al 2005) and the variability of feeding RNAi
457 knockdowns as compared to null mutant strains (Tavernarakis, Driscoll et al 2000), it seems likely that
458 our significant decreases in SYS-1 centrosomal recruitment represent either an intermediate knockdown
459 phenotype – the ideal hypomorphy between the extremes of catastrophic defects in spindle assembly
460 and organisms insufficiently affected to demonstrate a phenotype – or indicate that there is partial
461 redundancy between the SYS-1 relevant functions of the dynein motor. Our *dhc-1(ts)* experiments
462 support either case by clearly demonstrating a thorough dynein knockdown able to completely
463 uncouple centrosomal SYS-1. Alternatively, there could be partial redundancy among auxiliary dynein
464 components for SYS-1 binding/processivity, a possibility suggested by our *dhc-1(ts)* data which showed
465 the most severe reductions in centrosomal SYS-1.

466 Why, then, do we observe an increase in centrosomal SYS-1 steady state upon either long term
467 lower dose nocodazole-mediated knockdowns of trafficking or by RNAi depletion of trafficking subunit
468 ECPS-1? In response to these data (fig 4), we propose the additional SYS-1 negative regulator trafficking
469 component to this model. Disrupting the trafficking of centrosomal SYS-1 negative regulators should
470 result in a previously unseen increase in centrosomal SYS-1 steady state while maintaining a similar
471 effect on downstream gene expression and cell fate decisions, as seen above (Fig. 4-8). However, the
472 dichotomy between most dynein depletions and that of ECPS-1 or nocodazole treatment suggests a

473 differential efficiency in trafficking or centrosomal capture rate between SYS-1 and its negative
474 regulators, such as the proteasome. Most disruptions to the dynein motor that reduce SYS-1
475 centrosomal accumulation, mediated by maternally fed RNAi, are consistent but incomplete due to their
476 requirement for oogenesis and early embryonic viability. This, therefore, should produce embryos
477 capable of forming wild type dynein complexes, but at a far reduced rate. These dynein-limited embryos
478 should therefore decrease the volume of SYS-1 capable to be trafficked while not preventing the
479 centrosomal localization of an occasional proteasome complex sufficient to enzymatically process the
480 decreased SYS-1 flux. Similarly, depletion of dynein function by *dhc-1(ts)* effectively depletes all dynein
481 function but can only do so for brief portions of mitosis without inducing mitotic spindle collapse.

482 While these depletions limit the volume of trafficking by limiting the number of properly
483 constructed dynein motors, they don't limit the ability of an individual, functional dynein motor to
484 traffic. The experimental conditions that increase the steady state of centrosomal SYS-1, Nocodazole
485 and *ecps-1(RNAi)*, instead limit the scope of dynein cargo trafficking. ECPS-1, putative adapter between
486 dynein and the proteasome, increases the steady state of both SYS-1 and additional centrosomal
487 proteasome target ZYG-1. This supports the conserved role of ECPS-1, and results in embryos that are
488 not inhibited for overall dynein function but limited in their ability to traffic proteasome. Nocodazole
489 treatment similarly does not directly affect the processivity of dynein complexes that form on the
490 comparatively limited microtubule network. However, it does severely affect the reach of the
491 microtubule network itself (Fig 4A). Our data therefore suggests that the proteasome requires less
492 continual reinforcement by microtubule-mediated trafficking but does require more extensive
493 microtubule formation than is allowed in our Nocodazole-treated embryos.

494 A role for trafficking in both SYS-1 and its regulatory components, then, suggests a differentially
495 maintained steady state interaction for the proteasome and centrosomal SYS-1. While SYS-1 is rapidly
496 and continuously trafficked, it is similarly rapidly processed by centrosomal proteasome. That is, the

497 apparently rapid processing of centrosomal SYS-1 also requires rapid dynein-mediated flux to maintain
498 its centrosomal steady state. Any disruption to dynein processivity will therefore allow SYS-1 enrichment
499 to be overcome by its centrosomal processing, reducing the SYS-1 CEI by slowing the transfer of SYS-1
500 from cytoplasm to centrosome for degradation. By comparison, the proteasome complex endures at
501 the centrosome and continually processes SYS-1. However, the mass of the multi-megadalton complex,
502 or requisite assembling all 30 members of the 26S proteasome in stoichiometrically relevant numbers
503 (Papaevgeniou and Chondrogianni, 2014), suggests a requirement for continuous and highly processive
504 dynein trafficking to ensure its establishment at the centrosome. Our proposed model therefore
505 predicts that short term or partial disruptions to the dynein motor (Fig 9, red inset) allow for the
506 eventual establishment of a centrosomal proteolysis pathway, which may affect both SYS-1 and
507 proteasome localization, but nevertheless result in decreasing steady state levels of centrosomal SYS-1
508 (and presumably other proteasome targets that require active trafficking) as occasional proteasome
509 centrosomal localization overcomes the impaired localization of SYS-1. Conversely, long term systemic
510 disruptions to microtubule-mediated motors like that seen in Nocodazole treatment may still capture
511 SYS-1 in their comparatively limited microtubule network, while being disproportionately deprived of
512 the larger proteasome complex (Fig 9, blue inset).

513 Our model that both SYS-1 and its regulators are trafficked was supported but the identification
514 of a trafficking component that affects one but not both arms of our trafficking model. Most of our
515 perturbations, generally affecting more core components of the dynein machinery, may exert their
516 effects by detaching SYS-1 from the motor or by sabotaging all function of the motor complex (Fig S3A).
517 However, the specificity of our two transport mechanisms was exhibited by one dynein-protein
518 interaction, via depletion of ECPS-1/the putative ECM29 subunit of the motor. Unlike the other subunits
519 presenting strong SYS-1 phenotypes, ECM29 has not yet been implicated in dynein function beyond its
520 adaptor role but has notable effects on proteasome localization and response to stress (Gorbea,

521 Rechsteiner et al 2010; Haratake, Chiba et al 2016). Because *ecps-1(RNAi)* phenocopies the centrosomal
522 GFP::SYS-1 accumulation seen in proteasome knockdown via *rpt-4(RNAi)* as well as microtubule network
523 disruption via Nocodazole treatment, we propose that these observations support a role for
524 proteasomal localization as well as function for proper centrosomal clearance of SYS-1 (Fig 9).

525 While this model and our experiments to test it have been largely centered on SYS-1/β-catenin,
526 many developmental and temporally regulated proteins are known to pass through the centrosome
527 (Vora and Phillips 2016; Brown, Welch et al 1994; Johnston, Kopito et al 1998; Huang and Raff 1999;
528 Reck-Peterson, Carter et al 2018), as the centrosomal proteasome is far from SYS-1-specific. It is not
529 unreasonable, then, to presume that other proteins may benefit from dynein trafficking to something as
530 short-lived and yet influential to daughter cell inheritance as the mitotic centrosome. Particularly early
531 in eukaryotic development, subtle changes in the inheritance of cell fate determinants like SYS-1 can
532 have a profound effect on the ability of an organism to respond to environmental insults. For example,
533 the asymmetric nuclear localization of SYS-1 indicative of differential cell fate has been shown to arise
534 early, less than 70 seconds after the establishing division (Baldwin and Phillips 2014; Vora and Phillips
535 2015). We therefore propose that an active dynein mediated trafficking, at least for cell fate
536 determinants like SYS-1, could provide a universal buffering against excessive inheritance and
537 consequentially rare but deleterious cell fate changes.

538 **Materials and Methods**

539 **Strains**

540 Strains were maintained on Op50-inoculated NGM plates at 15° (BTP51, BTP220) or 25° C
541 (TX964, BTP51, LP563, TX691) using typical *C. elegans* methods. These strains contained the following
542 transgenes and alleles: **N2** (wild type); **TX964** (unc-119(ed3) III; him-3(e1147) IV; teis98 [Ppie-
543 1::GFP::SYS-1]); **BTP51** (unc-119(ed3) III; tjIs71 [pie-1 promoter::mCherry::H2B, pie-1 promoter::2x

544 mCherry::tbg-1, unc-119(+)]; qIs95 III) ; **BTP220** (unc-119(ed3) III; tjIs71 [pie-1 promoter::mCherry::H2B,

545 pie-1 promoter::2x mCherry::tbg-1, unc-119(+)]; qIs95 III; dhc-1(or195) I.) ; **TX691** (unc-119(ed3) III;

546 teIs46 [pRL1417; end-1p::GFP::H2B + unc-119(+)]) ; **OC341 (**unc-119(ed3) III; bsIs8[pMS5.1:unc -119(+)

547 pie -1- gfp-zyg-1C-terminus]); **BTP93** (*wIs78[SCMp::GFP + ajm-1p::GFP + F58E10* (cosmid) *+ unc-119(+*)]

548 *IV; uiwEx22*[*pHS::sys-1*]); **BTP97** (*qIs56[lag-2p::GFP + unc-119(+)] V;uiwIs3[pHS::sys-1*]); **AZ235** (*unc-*

549 *119(ed3) III; ruIs48[Ppie-1::gfp::tbb-1*];

550 **RNAi**

551 To perform RNAi knockdown of target genes, we used HT115 bacteria containing the pL4440

552 plasmid with a T7-flanked target gene insert. Most of these were obtained from a library supplied by

553 Ahringer (Kamath and Ahringer 2003). Those which were otherwise obtained (dlc-1) used target gene-

554 flanking primers with *C. elegans* cDNA to generate a new insert. These bacteria were used to seed IPTG-

555 containing, inducing plates as described previously. Worms were generally plated to RNAi after Sodium

556 Hypochlorite Synchronization as L1's. More deleterious knockdowns (*dlc-1, dhc-1)* were washed from

557 OP50 plates at 24 hours before imaging (L3/L4) or 12 hours before imaging (late L4/early adult)

558 (Timmons 2006; Bekas and Phillips 2020). DLC-1 WAS DERIVED USING RT PRIMERS DIGESTED WITH Xho I

559 and HIND III SEQUENCING 7/31

560 **Compound Microscopy, CEI, and Image Processing**

561 To obtain samples, mothers were anesthetized with 250 µM levamisole and dissected *via* a

562 clean surgical blade. Embryos were then transferred to a 2% agarose pad and imaged on a Zeiss Axio

563 Imager.D2. All exposure times were kept constant. Images were exported as uncompressed TIF's, and

564 fluorescence intensity was determined by measuring the mean fluorescence of centrosomal puncta in

565 ImageJ. The mean intensity of the remaining embryonic cytoplasm was subtracted from the centrosomal

566 mean to produce the CEI measurement, and identical measurements on 2x mCherry::tbg-1 were used

567 for TEI. END-1 family nuclei were assayed via the TX691 strain. GFP-tagged Histone intensity was
568 measured relative to the cytoplasmic autofluorescence.

569 **Temperature Sensitive Allele Imaging**

570 BTP51 and BTP220 were maintained together at 15°C and were imaged as above. Ambient
571 temperature in the microscope room was decreased to ~18°C for 'permissive' imaging and upshifted to
572 'restrictive' 26°C by moving slides to a Pecon Tempcontroller 2000-2 heated stage. Embryos were
573 imaged at the two temperatures sequentially, with approx. 45 seconds between upshift and image, or
574 were imaged as populations at either the permissive or restrictive temperature.

575 **Nocodazole Treatment**

576 In order to treat embryos before formation of the drug-impermeable eggshell, we exposed late
577 L4's to a low dose (approx. 83 μM, 25 μg/mL) nocodazole dissolved in 2% DMSO for 16 hours. Organisms
578 were then harvested by one minute centrifugation at 1000xG and imaged as described above.

579 **Confocal Microscopy and Fluorescence Recovery After Photobleach**

580 Confocal microscopy was performed via a Leica SP8 HyD detector system. The objective used
581 was a 63x HC PL APO CS2 objective with N.A. = 1.4, utilizing type F immersion oil. Each image analyzed
582 consisted of the sum of 35 z-images across the embryo, each slice approximately 0.35 μM thick. FRAP
583 was performed on the same system. Each embryo was imaged twice before bleaching, beginning as
584 soon as possible after NEBD. The ROI, an approximately 5μm square, was then bleached at an
585 intermediate focal plane with 100% laser power for 100 iterations. Images were taken as above, once
586 every 7 seconds. Fluorescence intensity was measured on summed slice Z-projections in FIJI via the
587 mean fluorescence intensity of ROIs drawn around relevant locales – either centrosome or the entire

588 dividing cell. Recovery was assayed by subtracting the ROI post-bleach intensity from each
589 measurement and evaluating it as a percentage of the pre-bleached centrosomal intensity.

590

591 **Heat Shock-Induced SYS-1 Overexpression**

592 BTP93 and BTP97 worms were exposed to brief 33°C heat shocks at relevant developmental
593 timepoints to drive SYS-1 overexpression concurrently with signaled cell fate specification. For DTCs,
594 BTP97 was subjected to 1-hour heat shock, 30-minutes recovery, and 30-minutes additional heat shock
595 beginning 11.5 hours after plating. For SCs, BTP93 was subjected to 2-hour heat shock, 30-minute
596 recovery, and additional 1-hour heat shock beginning 26 hours after plating. Both tissue types were
597 assayed 50 hours after plating.

598 **Acknowledgements**

599 We thank Kimberley Bekas and Amy Clemons for helpful comments on the manuscript. Strains
600 were provided by the Caenorhabditis Genetics Center, which is funded by the National Institutes of
601 Health (NIH) Office of Research Infrastructure Programs [P40 OD01440] and Dr. Kevin F. O'Connell at the
602 NIDDK (OC341). This work was supported by NIH award NIH GM114007 (B.T.P.).

603

604

605
606

607

608

609 **References**

610 Amsterdam, A., F. Pitzer and W. Baumeister, 1993 Changes in intracellular localization of proteasomes in
611 immortalized ovarian granulosa cells during mitosis associated with a role in cell cycle control.
612 Proc Natl Acad Sci U S A 90: 99-103.

613 Baldin, V., M. Militello, Y. Thomas, C. Doucet, W. Fic *et al.*, 2008 A novel role for PA28gamma-
614 proteasome in nuclear speckle organization and SR protein trafficking. Mol Biol Cell 19: 1706-
615 1716.

616 Baldwin, A. T., A. M. Clemons and B. T. Phillips, 2016 Unique and redundant beta-catenin regulatory
617 roles of two Dishevelled paralogs during C. elegans asymmetric cell division. J Cell Sci 129: 983-
618 993.

619 Baldwin, A. T., and B. T. Phillips, 2014 The tumor suppressor APC differentially regulates multiple beta-
620 catenins through the function of axin and CKIalpha during C. elegans asymmetric stem cell
621 divisions. J Cell Sci 127: 2771-2781.

622 Baldwin, A. T., and B. T. Phillips, 2018 Chapter 3 - Cell Polarity and Asymmetric Cell Division by the Wnt
623 Morphogen, pp. 61-102 in *Cell Polarity in Development and Disease*, edited by P. Michael Conn.
624 Academic Press, Boston.

625 Bei, Y., J. Hogan, L. A. Berkowitz, M. Soto, C. E. Rocheleau *et al.*, 2002 SRC-1 and Wnt signaling act
626 together to specify endoderm and to control cleavage orientation in early C. elegans embryos.
627 Dev Cell 3: 113-125.

628 Bekas, K. N., and B. T. Phillips, 2020 Generating reliable hypomorphic phenocopies by RNAi using long
629 dsRNA as diluent. MicroPubl Biol 2020.

630 Ben-Yaakov, K., S. Y. Dagan, Y. Segal-Ruder, O. Shalem, D. Vuppalanchi *et al.*, 2012 Axonal transcription
631 factors signal retrogradely in lesioned peripheral nerve. EMBO J 31: 1350-1363.

632 Bullock, S. L., and D. Ish-Horowicz, 2001 Conserved signals and machinery for RNA transport in
633 Drosophila oogenesis and embryogenesis. Nature 414: 611-616.
634 Carminati, J. L., and T. Stearns, 1997 Microtubules orient the mitotic spindle in yeast through dynein-
635 dependent interactions with the cell cortex. J Cell Biol 138: 629-641.
636 Chesney, M. A., N. Lam, D. E. Morgan, B. T. Phillips and J. Kimble, 2009 C. elegans HLH-2/E/Daughterless
637 controls key regulatory cells during gonadogenesis. Dev Biol 331: 14-25.
638 del Castillo, U., M. Winding, W. Lu and V. I. Gelfand, 2015 Interplay between kinesin-1 and cortical
639 dynein during axonal outgrowth and microtubule organization in Drosophila neurons. Elife 4:
640 e10140.
641 Deshimaru, M., M. Kinoshita-Kawada, K. Kubota, T. Watanabe, Y. Tanaka *et al.*, 2021 DCTN1 Binds to
642 TDP-43 and Regulates TDP-43 Aggregation. Int J Mol Sci 22.
643 Fabunmi, R., W. Wigley, P. Thomas and G. DeMartino, 2000 Activity and Regulation of the Centrosome-
644 associated Proteasome. Journal of Biological Chemistry 275: 409-413.
645 Fan, J., Q. Zhang, H. Tochio, M. Li and M. Zhang, 2001 Structural basis of diverse sequence-dependent
646 target recognition by the 8 kDa dynein light chain. J Mol Biol 306: 97-108.
647 Fuchs, E., and T. Chen, 2013 A matter of life and death: self-renewal in stem cells. EMBO Rep 14: 39-48.
648 Gao, F. J., L. Shi, T. Hines, S. Hebbar, K. L. Neufeld and D. S. Smith (2017). "Insulin signaling regulates a
649 functional interaction between adenomatous polyposis coli and cytoplasmic dynein." Mol Biol
650 Cell 28(5): 587-599.
651 Geyer, F. C., M. Lacroix-Triki, K. Savage, M. Arnedos, M. B. Lambros *et al.*, 2011 beta-Catenin pathway
652 activation in breast cancer is associated with triple-negative phenotype but not with CTNNB1
653 mutation. Mod Pathol 24: 209-231.
654 Gómez-López, S., R. G. Lerner and C. Petritsch, 2014 Asymmetric cell division of stem and progenitor
655 cells during homeostasis and cancer. Cell Mol Life Sci 71: 575-597.

656 Gorbea, C., G. Pratt, V. Ustrell, R. Bell, S. Sahasrabudhe *et al.*, 2010 A protein interaction network for
657 Ecm29 links the 26 S proteasome to molecular motors and endosomal components. J Biol Chem
658 285: 31616-31633.
659 Hames, R. S., R. E. Crookes, K. R. Straatman, A. Merdes, M. J. Hayes *et al.*, 2005 Dynamic recruitment of
660 Nek2 kinase to the centrosome involves microtubules, PCM-1, and localized proteasomal
661 degradation. Mol Biol Cell 16: 1711-1724.
662 Hamill, D. R., A. F. Severson, J. C. Carter and B. Bowerman, 2002 Centrosome maturation and mitotic
663 spindle assembly in C. elegans require SPD-5, a protein with multiple coiled-coil domains. Dev
664 Cell 3: 673-684.
665 Hanz, S., E. Perlson, D. Willis, J. Q. Zheng, R. Massarwa *et al.*, 2003 Axoplasmic importins enable
666 retrograde injury signaling in lesioned nerve. Neuron 40: 1095-1104.
667 Harada, A., Y. Takei, Y. Kanai, Y. Tanaka, S. Nonaka *et al.*, 1998 Golgi vesiculation and lysosome
668 dispersion in cells lacking cytoplasmic dynein. J Cell Biol 141: 51-59.
669 Haratake, K., A. Sato, F. Tsuruta and T. Chiba, 2016 KIAA0368-deficiency affects disassembly of 26S
670 proteasome under oxidative stress condition. J Biochem 159: 609-618.
671 He, T. C., A. B. Sparks, C. Rago, H. Hermeking, L. Zawel *et al.*, 1998 Identification of c-MYC as a target of
672 the APC pathway. Science 281: 1509-1512.
673 Horgan, C. P., S. R. Hanscom, R. S. Jolly, C. E. Futter and M. W. McCaffrey, 2010 Rab11-FIP3 links the
674 Rab11 GTPase and cytoplasmic dynein to mediate transport to the endosomal-recycling
675 compartment. J Cell Sci 123: 181-191.
676 Huang, L., D. Pike, D. E. Sleat, V. Nanda and P. Lobel, 2014 Potential pitfalls and solutions for use of
677 fluorescent fusion proteins to study the lysosome. PLoS One 9: e88893.

678 Huang, S., P. Shetty, S. M. Robertson and R. Lin, 2007 Binary cell fate specification during C. elegans
679 embryogenesis driven by reiterated reciprocal asymmetry of TCF POP-1 and its coactivator beta-
680 catenin SYS-1. Development 134: 2685-2695.
681 Hutagalung, A. H., and P. J. Novick, 2011 Role of Rab GTPases in membrane traffic and cell physiology.
682 Physiol Rev 91: 119-149.
683 Jha, R., and T. Surrey, 2015 Regulation of processive motion and microtubule localization of cytoplasmic
684 dynein. Biochem Soc Trans 43: 48-57.
685 Juanes, M. A., 2020 Cytoskeletal Control and Wnt Signaling-APC's Dual Contributions in Stem Cell
686 Division and Colorectal Cancer. Cancers (Basel) 12.
687 Kamath, R. S., A. G. Fraser, Y. Dong, G. Poulin, R. Durbin *et al.*, 2003 Systematic functional analysis of the
688 Caenorhabditis elegans genome using RNAi. Nature 421: 231-237.
689 Kawaguchi, Y., J. J. Kovacs, A. McLaurin, J. M. Vance, A. Ito *et al.*, 2003 The deacetylase HDAC6 regulates
690 aggresome formation and cell viability in response to misfolded protein stress. Cell 115: 727-
691 738.
692 Kidd, A. R., 3rd, J. A. Miskowski, K. R. Siegfried, H. Sawa and J. Kimble, 2005 A beta-catenin identified by
693 functional rather than sequence criteria and its role in Wnt/MAPK signaling. Cell 121: 761-772.
694 Lam, A. K., and B. T. Phillips, 2017 Wnt Signaling Polarizes C. elegans Asymmetric Cell Divisions During
695 Development. Results Probl Cell Differ 61: 83-114.
696 Leduc, C., K. Padberg-Gehle, V. Varga, D. Helbing, S. Diez *et al.*, 2012 [How to avoid the formation of
697 molecular motors traffic jam during intracellular transport]. Med Sci (Paris) 28: 1064-1066.
698 Leggett, D. S., J. Hanna, A. Borodovsky, B. Crosas, M. Schmidt *et al.*, 2002 Multiple associated proteins
699 regulate proteasome structure and function. Mol Cell 10: 495-507.

700 Liu, W., X. Dong, M. Mai, R. S. Seelan, K. Taniguchi *et al.*, 2000 Mutations in AXIN2 cause colorectal
701 cancer with defective mismatch repair by activating beta-catenin/TCF signalling. Nat Genet 26:
702 146-147.
703 Mbom, B. C., K. A. Siemers, M. A. Ostrowski, W. J. Nelson and A. I. Barth, 2014 Nek2 phosphorylates and
704 stabilizes beta-catenin at mitotic centrosomes downstream of Plk1. Mol Biol Cell 25: 977-991.
705 Mikenberg, I., D. Widera, A. Kaus, B. Kaltschmidt and C. Kaltschmidt, 2007 Transcription factor NF-
706 kappaB is transported to the nucleus via cytoplasmic dynein/dynactin motor complex in
707 hippocampal neurons. PLoS One 2: e589.
708 Mila, D., A. Calderon, A. T. Baldwin, K. M. Moore, M. Watson *et al.*, 2015 Asymmetric Wnt Pathway
709 Signaling Facilitates Stem Cell-Like Divisions via the Nonreceptor Tyrosine Kinase FRK-1 in
710 Caenorhabditis elegans. Genetics 201: 1047-1060.
711 Miskowski, J., Y. Li and J. Kimble, 2001 The sys-1 gene and sexual dimorphism during gonadogenesis in
712 Caenorhabditis elegans. Dev Biol 230: 61-73.
713 Niehrs, C., and S. P. Acebron, 2012 Mitotic and mitogenic Wnt signalling. EMBO J 31: 2705-2713.
714 Niehrs, C., and S. P. Acebron, 2012 Mitotic and mitogenic Wnt signalling. EMBO J 31: 2705-2713.
715 Nusse, R., and H. Clevers, 2017 Wnt/beta-Catenin Signaling, Disease, and Emerging Therapeutic
716 Modalities. Cell 169: 985-999.
717 O'Connell, K. F., C. Caron, K. R. Kopish, D. D. Hurd, K. J. Kemphues *et al.*, 2001 The C. elegans zyg-1 gene
718 encodes a regulator of centrosome duplication with distinct maternal and paternal roles in the
719 embryo. Cell 105: 547-558.
720 O'Rourke, S. M., M. D. Dorfman, J. C. Carter and B. Bowerman, 2007 Dynein modifiers in C. elegans: light
721 chains suppress conditional heavy chain mutants. PLoS Genet 3: e128.

722 Peel, N., M. Dougherty, J. Goeres, Y. Liu and K. F. O'Connell, 2012 The C. elegans F-box proteins LIN-23
723 and SEL-10 antagonize centrosome duplication by regulating ZYG-1 levels. J Cell Sci 125: 3535-
724 3544.
725 Peters, N., D. E. Perez, M. H. Song, Y. Liu, T. Muller-Reichert *et al.*, 2010 Control of mitotic and meiotic
726 centriole duplication by the Plk4-related kinase ZYG-1. J Cell Sci 123: 795-805.
727 Phillips, B. T., A. R. Kidd, 3rd, R. King, J. Hardin and J. Kimble, 2007 Reciprocal asymmetry of SYS-1/beta-
728 catenin and POP-1/TCF controls asymmetric divisions in Caenorhabditis elegans. Proc Natl Acad
729 Sci U S A 104: 3231-3236.
730 Pintard, L., and B. Bowerman, 2019 Mitotic Cell Division in Caenorhabditis elegans. Genetics 211: 35-73.
731 Pinto, D., A. Gregorieff, H. Begthel and H. Clevers, 2003 Canonical Wnt signals are essential for
732 homeostasis of the intestinal epithelium. Genes Dev 17: 1709-1713.
733 Priyanga, J., G. Guha and D. Bhakta-Guha, 2021 Microtubule motors in centrosome homeostasis: A
734 target for cancer therapy? Biochim Biophys Acta Rev Cancer 1875: 188524.
735 Reck-Peterson, S. L., W. B. Redwine, R. D. Vale and A. P. Carter, 2018 The cytoplasmic dynein transport
736 machinery and its many cargoes. Nat Rev Mol Cell Biol 19: 382-398.
737 Reilein, A., D. Melamed, K. S. Park, A. Berg, E. Cimetta *et al.*, 2017 Alternative direct stem cell derivatives
738 defined by stem cell location and graded Wnt signalling. Nat Cell Biol 19: 433-444.
739 Reya, T., and H. Clevers, 2005 Wnt signalling in stem cells and cancer. Nature 434: 843-850.
740 Sawa, H., 2012 Control of cell polarity and asymmetric division in C. elegans. Curr Top Dev Biol 101: 55-
741 76.
742 Schmidt, R., L. E. Fielmich, I. Grigoriev, E. A. Katrukha, A. Akhmanova *et al.*, 2017 Two populations of
743 cytoplasmic dynein contribute to spindle positioning in C. elegans embryos. J Cell Biol 216: 2777-
744 2793.

745 Shtutman, M., J. Zhurinsky, I. Simcha, C. Albanese, M. D'Amico *et al.*, 1999 The cyclin D1 gene is a target
746 of the beta-catenin/LEF-1 pathway. Proc Natl Acad Sci U S A 96: 5522-5527.
747 Siegfried, K. R., A. R. Kidd, M. A. Chesney and J. Kimble, 2004 The sys-1 and sys-3
748 Genes Cooperate With Wnt Signaling to Establish the Proximal-Distal Axis of the
749 Caenorhabditis elegans Gonad. Genetics 166: 171-186.
750 Sonnichsen, B., L. B. Koski, A. Walsh, P. Marschall, B. Neumann *et al.*, 2005 Full-genome RNAi profiling of
751 early embryogenesis in Caenorhabditis elegans. Nature 434: 462-469.
752 Sugioka, K., K. Mizumoto and H. Sawa, 2011 Wnt regulates spindle asymmetry to generate asymmetric
753 nuclear beta-catenin in C. elegans. Cell 146: 942-954.
754 Sunchu, B., and C. Cabernard, 2020 Principles and mechanisms of asymmetric cell division. Development
755 147.
756 Tame, M. A., J. A. Raaijmakers, B. van den Broek, A. Lindqvist, K. Jalink *et al.*, 2014 Astral microtubules
757 control redistribution of dynein at the cell cortex to facilitate spindle positioning. Cell Cycle 13:
758 1162-1170.
759 Tavernarakis, N., S. L. Wang, M. Dorovkov, A. Ryazanov and M. Driscoll, 2000 Heritable and inducible
760 genetic interference by double-stranded RNA encoded by transgenes. Nat Genet 24: 180-183.
761 Tejpar, S., F. Nollet, C. Li, J. S. Wunder, G. Michils *et al.*, 1999 Predominance of beta-catenin mutations
762 and beta-catenin dysregulation in sporadic aggressive fibromatosis (desmoid tumor). Oncogene
763 18: 6615-6620.
764 Tetsu, O., and F. McCormick, 1999 Beta-catenin regulates expression of cyclin D1 in colon carcinoma
765 cells. Nature 398: 422-426.
766 Timmons, L., 2006 Delivery methods for RNA interference in C. elegans. Methods Mol Biol 351: 119-125.

767 Valenzuela, J. I., M. Jaureguiberry-Bravo, D. A. Salas, O. A. Ramírez, V. H. Cornejo *et al.*, 2014 Transport
768 along the dendritic endoplasmic reticulum mediates the trafficking of GABAB receptors. J Cell Sci
769 127: 3382-3395.
770 Vora, S., and B. T. Phillips, 2015 Centrosome-Associated Degradation Limits beta-Catenin Inheritance by
771 Daughter Cells after Asymmetric Division. Curr Biol 25: 1005-1016.
772 Vora, S. M., J. S. Fassler and B. T. Phillips, 2020 Centrosomes are required for proper beta-catenin
773 processing and Wnt response. Mol Biol Cell 31: 1951-1961.
774 Vora, S. M., and B. T. Phillips, 2016 The benefits of local depletion: The centrosome as a scaffold for
775 ubiquitin-proteasome-mediated degradation. Cell Cycle 15: 2124-2134.
776 Wigley, W. C., R. P. Fabunmi, M. G. Lee, C. R. Marino, S. Muallem *et al.*, 1999 Dynamic association of
777 proteasomal machinery with the centrosome. J Cell Biol 145: 481-490.
778 Wójcik, C., and G. N. DeMartino, 2003 Intracellular localization of proteasomes. The International
779 Journal of Biochemistry & Cell Biology 35: 579-589.
780 Wozniak, M. J., B. Bola, K. Brownhill, Y. C. Yang, V. Levakova *et al.*, 2009 Role of kinesin-1 and
781 cytoplasmic dynein in endoplasmic reticulum movement in VERO cells. J Cell Sci 122: 1979-1989.
782 Wühr, M., E. S. Tan, S. K. Parker, H. W. Detrich, 3rd and T. J. Mitchison, 2010 A model for cleavage plane
783 determination in early amphibian and fish embryos. Curr Biol 20: 2040-2045.
784 Yang, L., X. Wu, Y. Wang, K. Zhang, J. Wu *et al.*, 2011 FZD7 has a critical role in cell proliferation in triple
785 negative breast cancer. Oncogene 30: 4437-4446.

786 Zhunussova, G., G. Afonin, S. Abdikerim, A. Jumanov, A. Perfilyeva *et al.*, 2019 Mutation Spectrum of
787 Cancer-Associated Genes in Patients With Early Onset of Colorectal Cancer. Front Oncol 9: 673.

788

789

790 **FIGURE LEGENDS**

791 **Figure 1:**

792 Graphical hypothesis and expected results. 1a) Two potential mechanisms by which SYS-1 (Green) is
793 recruited to centrosomes. We will distinguish approximately the proportion of SYS-1 actively localized by
794 motor trafficking (indicated by yellow, blue, and purple complex along black microtubules), or passively
795 via diffusion-capture (indicated by dashed blue lines). 1B-D) Expected outcomes for centrosomal
796 recruitment of SYS-1 (top), daughter cell nuclear SYS-1 enrichment (middle), and cell fate (bottom) in
797 wild type (b) organisms with disrupted SYS-1 centrosomal enrichment (c) and organisms which have
798 disrupted centrosomal negative regulation of SYS-1 (d). Increasing SYS-1 nuclear enrichment in daughter
799 cells is indicated by darker shade of green color, while darker orange and blue shade indicates the
800 robustness of corresponding signaled and unsignaled cell fates, respectively

801 **Figure 2:**

802 Rationale and methodology for microtubule motor RNAi Screen. A) GFP::SYS-1 can be occasionally
803 observed at regions corresponding to DHC-1 mitotic accumulation. This is particularly enhanced in
804 centrosomally uncoupled *rsa-2(RNAi)* organisms. The frequency of GFP::SYS-1 enrichment at these
805 locales in lacZ(RNAi) and rsa-2(RNAi) treatment is distinguished by color. A') GFP::SYS-1 at kinetochore
806 microtubule (white arrowhead) and cortex(black arrowhead) of the dividing *C. elegans* early embryo.
807 Inset in black shows cortical localization with increased contrast.. B) Demonstration of CEI and TEI
808 calculation. CEI was calculated in FIJI by subtracting the mean pixel intensity of a cytoplasmic ROI
809 encompassing the proximal half of the dividing cell, approximated by the light blue square, from a
810 circular centrosome ROI, approximated by the white square. B') Expanded view of ROI's as defined in B.
811 B'') Graphical representation of the raw centrosomal and CEI adjusted fluorescence intensity for the

812 control (Left) and Affected (right) embryos in B. Control (*lacZ(RNAi)* treated) exhibits both a high raw
813 centrosomal GFP::SYS-1 and CEI. Affected (*rsa-2(RNAi)* treated) exhibits an intermediate raw GFP::SYS-1,
814 but severely decreased CEI, better reflecting its visual failure to increase centrosomal GFP::SYS-1 notably
815 above the bulk of cytoplasmic representation. C) Example YFP::SYS-1 CEI (C) and CEI/TEI (C') of controls
816 and indicated dynein light chain depletions. Width of the violin plot corresponds to a histogram of
817 observation density. The median is indicated by the central white dot, with the interquartile range
818 indicated by the thick black line, and 1.5x additional Interquartile range indicated by the thin black line.
819 N= lacZ(RNAi), 72; *dlc-1(RNAi),* 74; *dylt-1(RNAi),* 52; *rsa-2(RNAi)*, 22 * - p<0.05, ** - p<0.01, *** - p<0.001
820 by Chi-square test (A) or Student's t-test (C-C').

821 **Figure 3:**

822 tsAllele mediated loss of dynein function has a disproportionate effect on SYS-1 localization. . A)
823 Diagram of the Dynein motor, and hypothetical model of its role in SYS-1 trafficking. Relative location of
824 *dhc-1(ts)* lesion indicated. B) Representative centrosome images of YFP::SYS-1 and g-Tubulin::mCherry in
825 wildtype and ts allele-containing organisms C) embryos at comparable cell cycle phase before (top) and
826 after (bottom) temperature upshift. D) SYS-1 CEI and D') SYS-1 CEI per TEI in organisms containing *dhc-*
827 *1(ts)* , to control for differences in centrosome assembly, standard error depicted. N= 44, 31, 38, 25 in D
828 and D' columns, left to right. * - p<0.05, ** - p<0.01, *** - p<0.001 by Student's t-test.

829 **Figure 4:**

830 Nocodazole mediated disruption of microtubules enhances centrosomal GFP::SYS-1 enrichment A)
831 Representative images of GFP::TBB-1 in DMSO and Nocodazole treated embryos. White arrowheads
832 indicate astral microtubules (left) and the corresponding lack or dysregulated region in nocodazole
833 treatment (right) B) Quantification of, and C) Representative images of similarly treated GFP::SYS-1

834 embryos. For B, N=36 DMSO and 46 nocodazole treated embryos. * - p<0.05, ** - p<0.01, *** - p<0.001

835 by Student's t-test. D) CEI/TEI as evaluated with combinatorial Wildtype (WT) or *dhc-1(ts)* allele for

836 Dynein Heavy Chain, and treatment with 2% DMSO vehicle media or 2% DMSO + nocodazole media.

837 Organisms at the permissive and restrictive temperature are differentiated by blue and red coloring,

838 respectively. Error bars are SEM. E) Representative yfp::SYS-1 and mCh::g-Tubulin for each treatment in

839 D, respectively.

840 **Figure 5:**

841 Microtubule-mediated processes can also stabilize centrosomal SYS-1. A) Treatment with *ecps-1(RNAi)*

842 enhances centrosomal SYS-1 accumulation, N=48 *lacZ(RNAi), N* =12 *rsa-2(RNAi), N*= 124 *ecps-1(RNAi).* B)

843 *lacZ(RNAi)* and *ecps-1(RNAi)* representative centrosomes in grayscale and intensity dependent LUT. C)

844 Putative dynein and proteasome adaptor ECPS-1 also appears to also enhance centrosomal ZYG-1

845 accumulation, by GFP::ZYG-1c CEI (N=31 untreated, N=19 *ecps-1(RNAi),* N= 20 *rpt-4(RNAi),* 14 *rsa-*

846 *2(RNAi*)) and D) Representative GFP::ZYG-1c centrosomal images in grayscale and intensity dependent

847 LUT. E) E) Quantified recovery of GFP::SYS-1. Values indicated are the ratio of bleached centrosomes to

848 their pre-bleach value, normalized such that the post-bleach value, t = 0, is 0 GFP::SYS-1 intensity. Error

849 bars are SEM. (F-F'') representative FRAP montage of 2nd division P1 cells in indicated embryos. Two

850 pre-bleach, immediately consecutive timepoints are followed by the 1st post-bleach image at time '0'

851 and images every 7 seconds thereafter indicated top left. * - p<0.05, ** - p<0.01, *** - p<0.001 by

852 Student's t-test. One-sided Student's T, asterisk indicates p-value from *lacZ(RNAi)* in E-F.

853 **Figure 6:**

854 Effect of Dynein Depletion on nuclear SYS-1 Localization and Gene Expression in EMS Descendant Cells.

855 A) The EMS precursor (embryo ventral cell) divides, receiving Wnt and Src specification and orientation

856 cues, respectively (red arrow). These daughters give rise to posterior, signaled E and anterior, unsignaled
857 MS daughter cells. Wildtype specification results in depicted approximate GFP::SYS-1 localization
858 pattern specifically enriched in the signaled daughter nucleus. B) Representative images of wildtype and
859 *ecps-1(RNAi)* treated embryos. Orange box encloses the unsignaled MS nucleus, Blue box encloses the
860 signaled E nucleus. C) Quantification of GFP::SYS-1 nuclear enrichment in indicated dynein RNAi
861 knockdowns. C') Mean difference in nuclear GFP::SYS-1 enrichment from quantification in C. Error bars
862 are SEM. D) Embryos ectopically expressing pEND-1::GFP::H2B in cells not descended from the E lineage
863 in the first (orange) second (blue) and third (green) lineage after the founding of the lineage (the 2, 4,
864 and 8 cell E descendants, respectively). D') Representative embryos exhibiting WT (all lacZ(RNAi)-
865 treated, left) and ectopic (*ecps-1(RNAi)*- and 2x*dhc-1(RNAi)*- treated for 1, 2, and 3 generations after E
866 founding, respectively, right) pEND-1::GFP::H2B

867 **Figure 7:**

868 SYS-1 dysregulation via dynein knockdown can cause rare cell fate conversions. A) Diagram of *C. elegans*
869 distal tip cell signaled lineage specification in the somatic gonadal precursor. B) Representative image of
870 WT (top) and ectopically induced (bottom) distal tip cells (DTCs). To distinguish DTC's from pLAG-2
871 driven vulval expression, DTCs are marked with white arrowheads. C) Number and relative frequency of
872 DTCs via anatomical marker in untreated organisms and in backgrounds with RNAi depletion of various
873 dynein subunits. D) Number and relative frequency of DTCs marked by anatomical marker when SYS-1 is
874 overexpressed via a heat shock-driven transgene in both untreated organisms and in backgrounds with
875 RNAi depletion of various dynein subunits. * = $p<0.05$, ** = $p<0.01$, *** = $p<0.001$ by one-sided Mann-
876 Whitney test

877 **Figure 8:**

878 SYS-1 dysregulation via dynein knockdown can cause rare cell fate conversions. A) Diagram of *C. elegans*
879 seam cell (SC) signaled lineage. B) Representative image of WT (top) and ectopically induced (bottom)
880 SCs. Likely ectopic SC exhibit spatially distinct 'doublets', highlighted here in brackets. C) Number and
881 relative frequency of SCs via anatomical marker when in untreated organisms and in backgrounds with
882 RNAi depletion of various dynein subunits. D) Number and relative frequency of SCs via anatomical
883 marker when SYS-1 is overexpressed via a heat shock-driven transgene in both untreated organisms and
884 in backgrounds with RNAi depletion of various dynein subunits. * = $p<0.05$, ** = $p<0.01$, *** = $p<0.001$
885 by Mann-Whitney test

886 **Figure 9:**

887 Model, demonstrating the various processes by which SYS-1 and its regulators appear to be localized to
888 mitotic centrosomes. Both SYS-1 and some component of its centrosomal proteasome-dependent
889 negative regulators, here represented by purple circle, demonstrate some dependence on microtubule
890 mediated trafficking. While various dynein subunits are requisite components of a functional dynein
891 complex, the negative effect of their depletion on SYS-1 centrosomal steady state indicates a
892 preferential or more frequent trafficking of SYS-1. Relatively rare proteasome trafficking events
893 mediated by ECPS-1 meanwhile, are sufficient to maintain appropriate SYS-1 centrosomal enrichment.
894 This less efficient proteasomal trafficking, however, renders it vulnerable to Nocodazole-mediated
895 decrease in overall microtubule trafficking/network formation efficiency. Red inset depicts decreased
896 processivity or cargo binding capacity induced by dynein light chain RNAi depletions. Blue inset depicts
897 depletion of adapter ECPS-1 and resulting depletion of proteasome-trafficking specific dynein
898 complexes, while not otherwise affecting the microtubule motor.

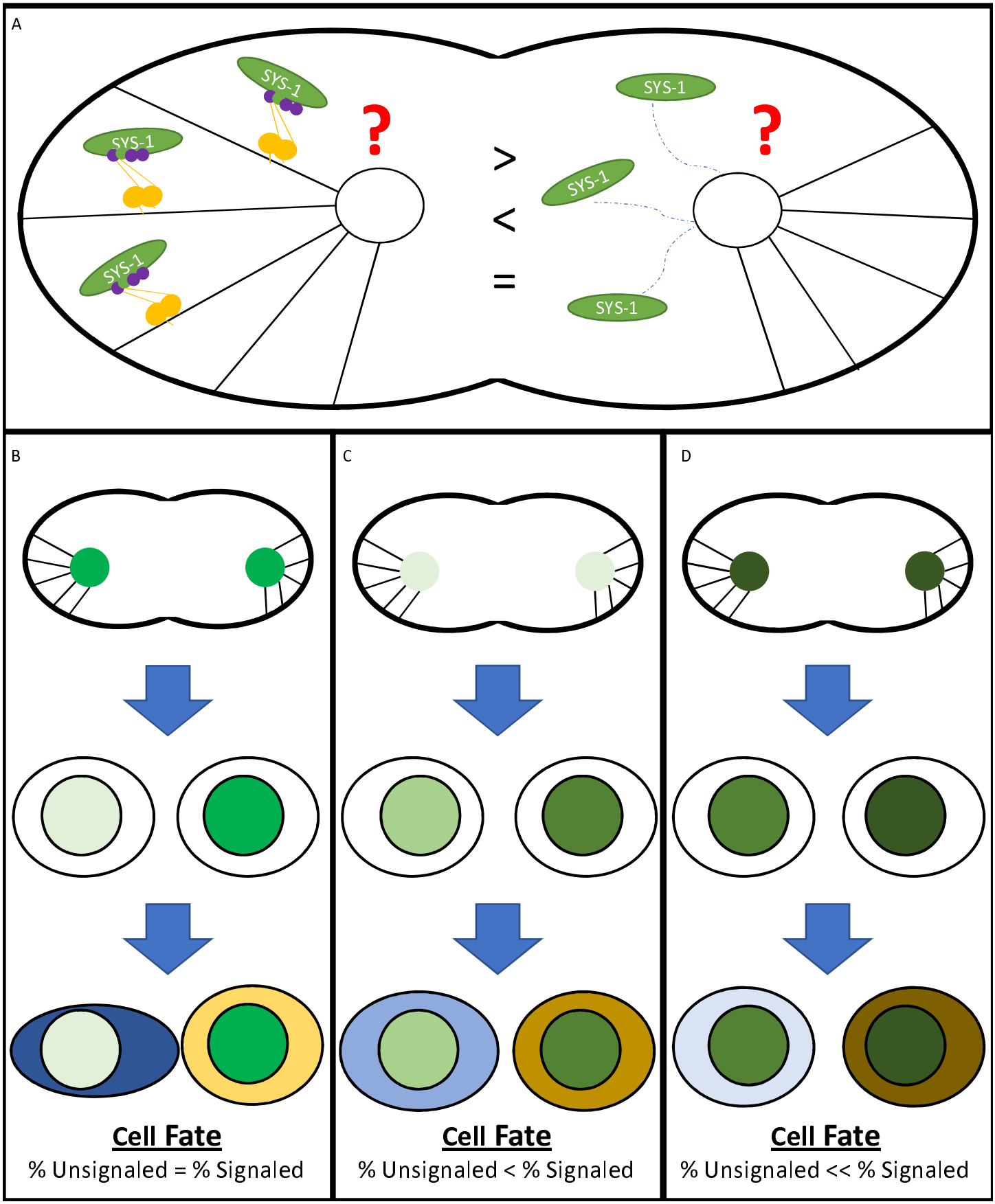
A
SYS-1
SYS-1
SYS-1
?
>
<
=
SYS-1
SYS-1
SYS-1
?
B
Cell Fate
% Unsignaled = % Signaled
C
Cell Fate
% Unsignaled < % Signaled
D
Cell Fate
% Unsignaled << % Signaled

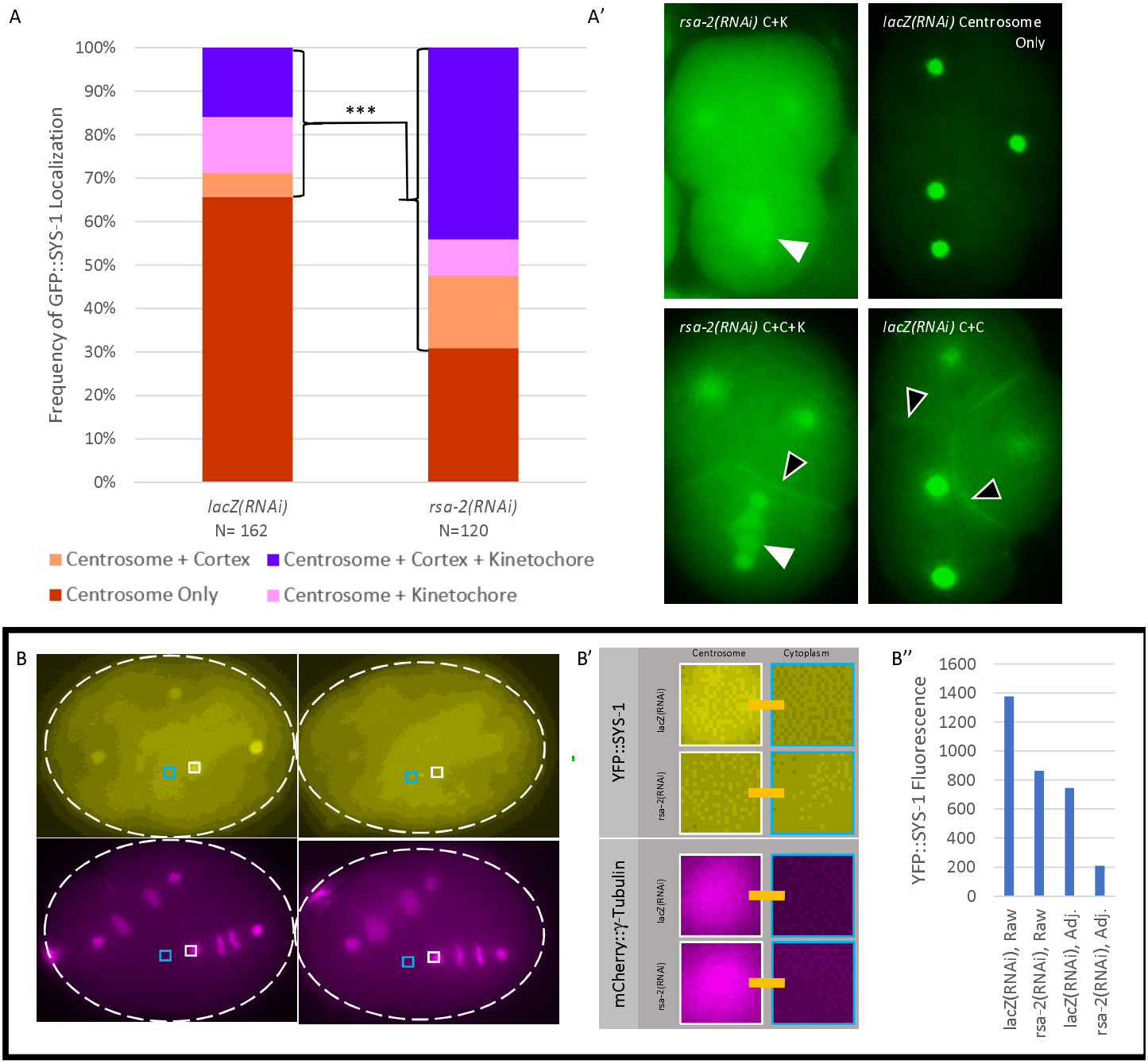
A
A'
Frequency of GFP::SYS-1 Localization
100%
90%
80%
70%
60%
50%
40%
30%
20%
10%
0%
***
lacZ(RNAi)
N= 162
rsa-2(RNAi)
N=120
Centrosome + Cortex
Centrosome + Cortex + Kinetochore
Centrosome Only
Centrosome + Kinetochore
rsa-2(RNAi) C+K
lacZ(RNAi) Centrosome Only
rsa-2(RNAi) C+C+K
lacZ(RNAi) C+C
B
B'
B''
Centrosome
Cytoplasm
YFP::SYS-1
mCherry::γ-Tubulin
lacZ(RNAi)
rsa-2(RNAi)
YFP::SYS-1 Fluorescence
1600
1400
1200
1000
800
600
400
200
0
lacZ(RNAi), Raw
rsa-2(RNAi), Raw
lacZ(RNAi), Adj.
rsa-2(RNAi), Adj.

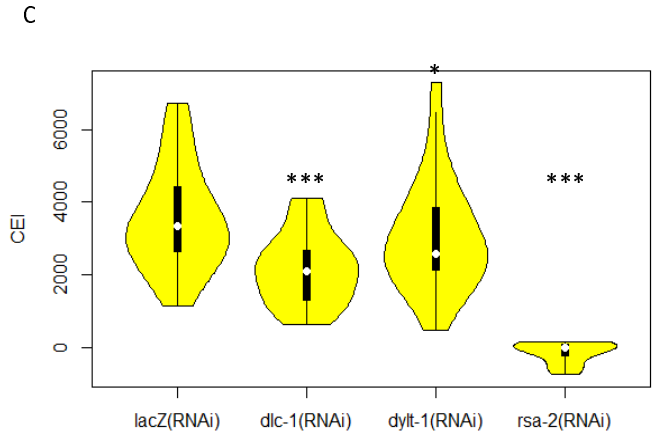
C
CEI
0
2000
4000
6000
*
***
***
lacZ(RNAi)
dlc-1(RNAi)
dylt-1(RNAi)
rsa-2(RNAi)

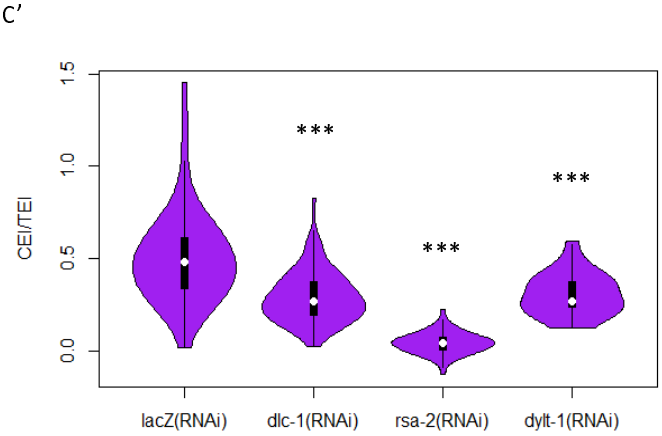
C'
CEI/TEI
0.0
0.5
1.0
1.5
***
***
***
lacZ(RNAi)
dlc-1(RNAi)
rsa-2(RNAi)
dylt-1(RNAi)

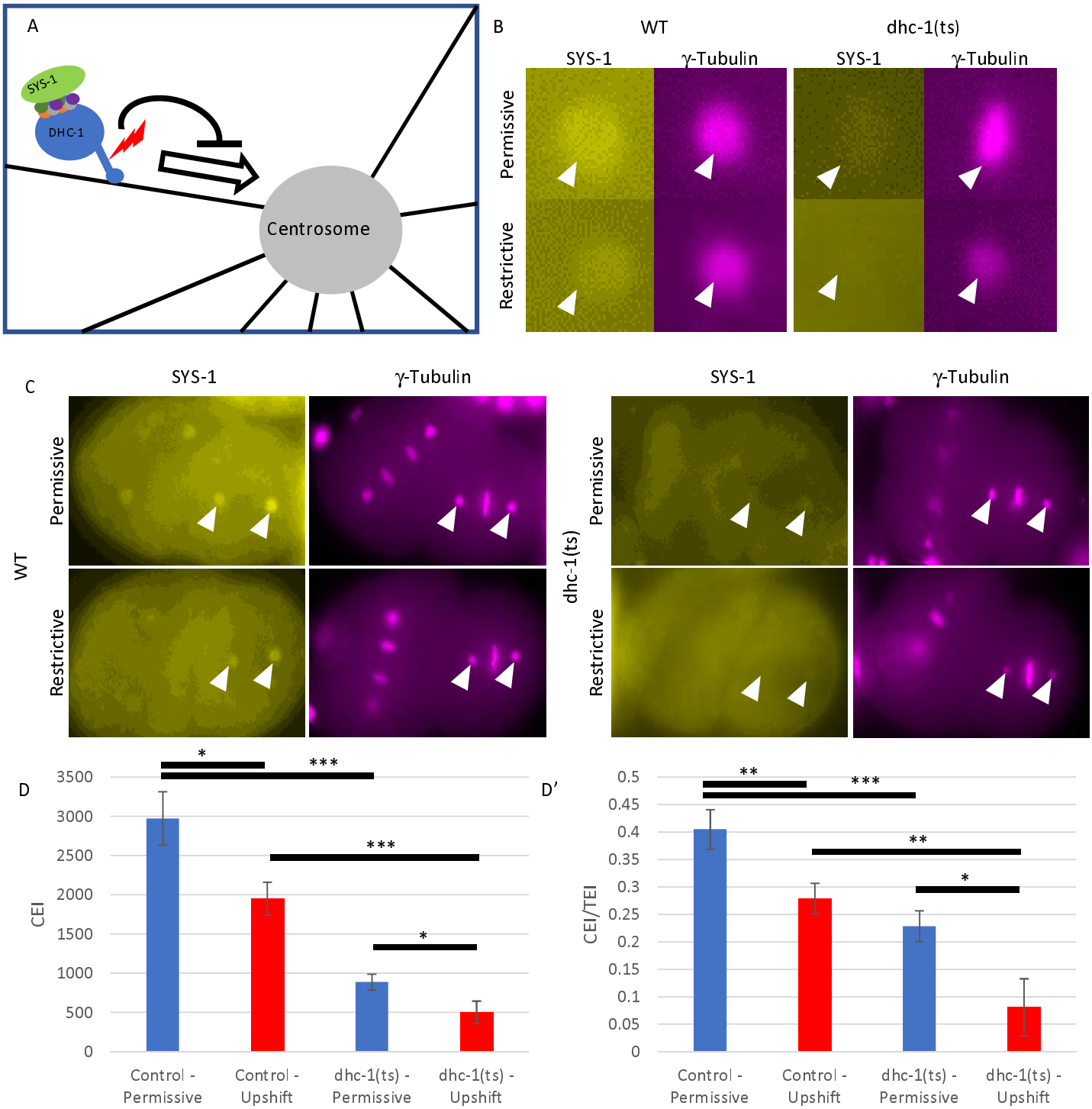
A
SYS-1
DHC-1
Centrosome
B
WT
dhc-1(ts)
SYS-1
γ-Tubulin
SYS-1
γ-Tubulin
Permissive
Restrictive
C
SYS-1
γ-Tubulin
SYS-1
γ-Tubulin
WT
dhc-1(ts)
Permissive
Restrictive
Permissive
Restrictive
D
CEI
3500
3000
2500
2000
1500
1000
500
0
*
***
***
*
Control - Permissive
Control - Upshift
dhc-1(ts) - Permissive
dhc-1(ts) - Upshift
D'
CEI/TEI
0.5
0.45
0.4
0.35
0.3
0.25
0.2
0.15
0.1
0.05
0
**
***
**
*
Control - Permissive
Control - Upshift
dhc-1(ts) - Permissive
dhc-1(ts) - Upshift

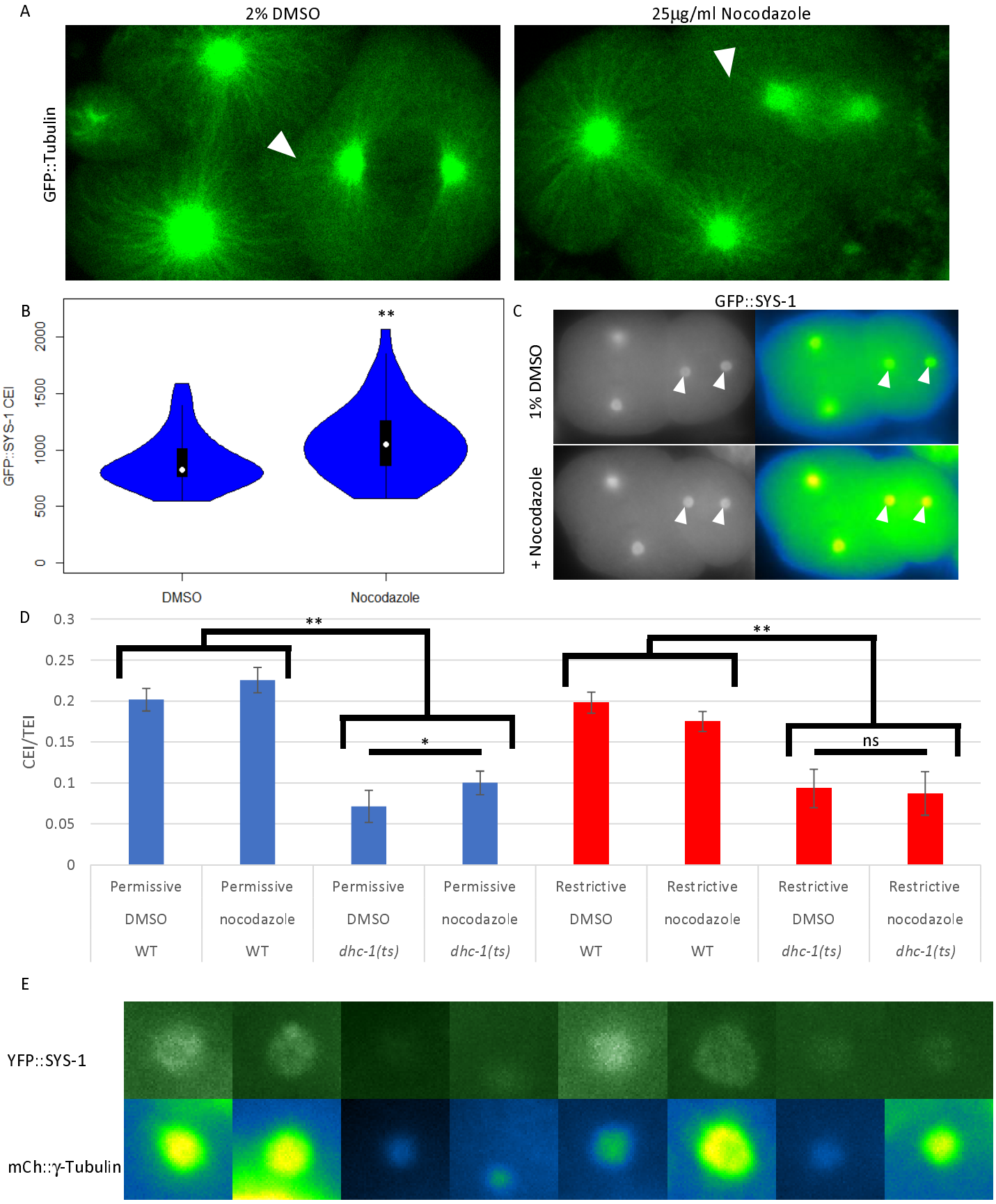
A
2% DMSO
25µg/ml Nocodazole
GFP::Tubulin
B
GFP::SYS-1 CEI
0
500
1000
1500
2000
**
DMSO
Nocodazole
C
GFP::SYS-1
1% DMSO
+ Nocodazole
D
CEI/TEI
0
0.05
0.1
0.15
0.2
0.25
0.3
**
*
**
ns
Permissive DMSO WT
Permissive nocodazole WT
Permissive DMSO dhc-1(ts)
Permissive nocodazole dhc-1(ts)
Restrictive DMSO WT
Restrictive nocodazole WT
Restrictive DMSO dhc-1(ts)
Restrictive nocodazole dhc-1(ts)
E
YFP::SYS-1
mCh::γ-Tubulin

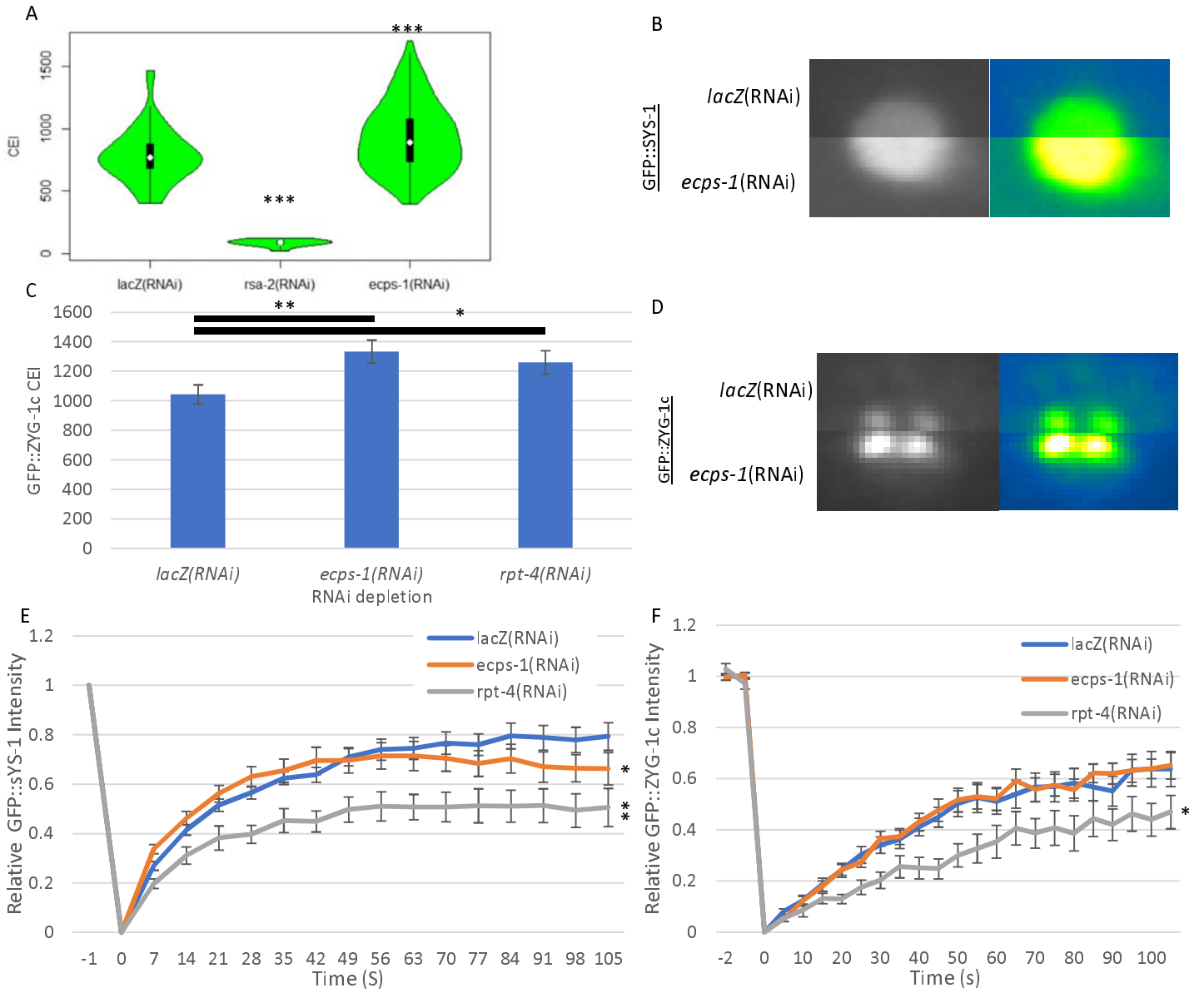

G – GFP::SYS-1 recovery in *lacZ(RNAi)*

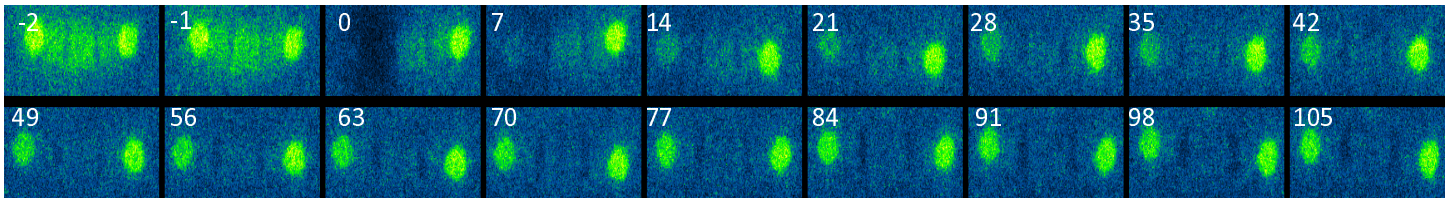

G' – GFP::SYS-1 recovery in *rpt-4(RNAi)*

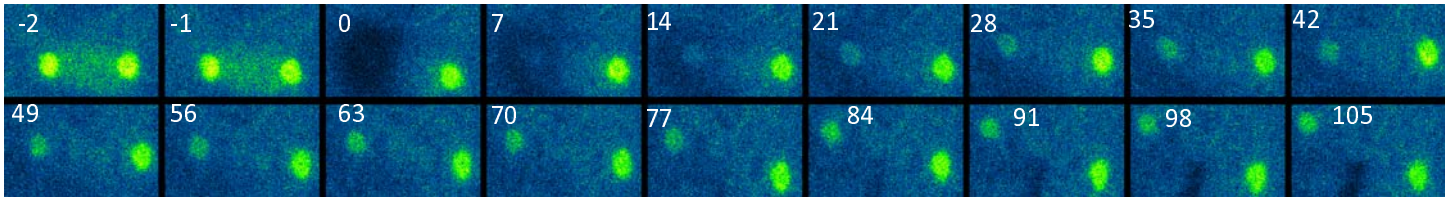

G'' – GFP::SYS-1 recovery in *ecps-1(RNAi)*

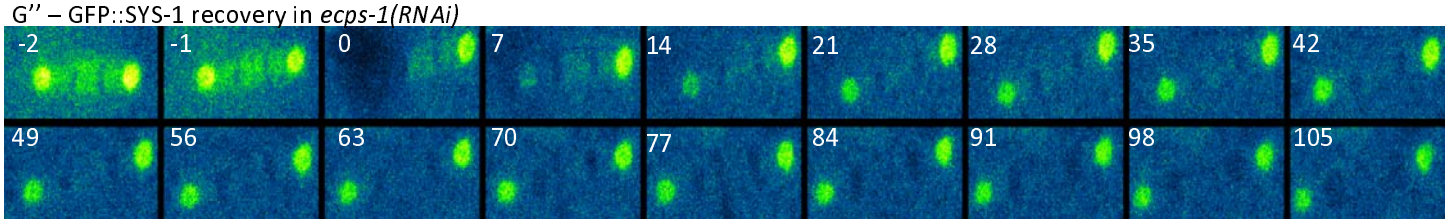

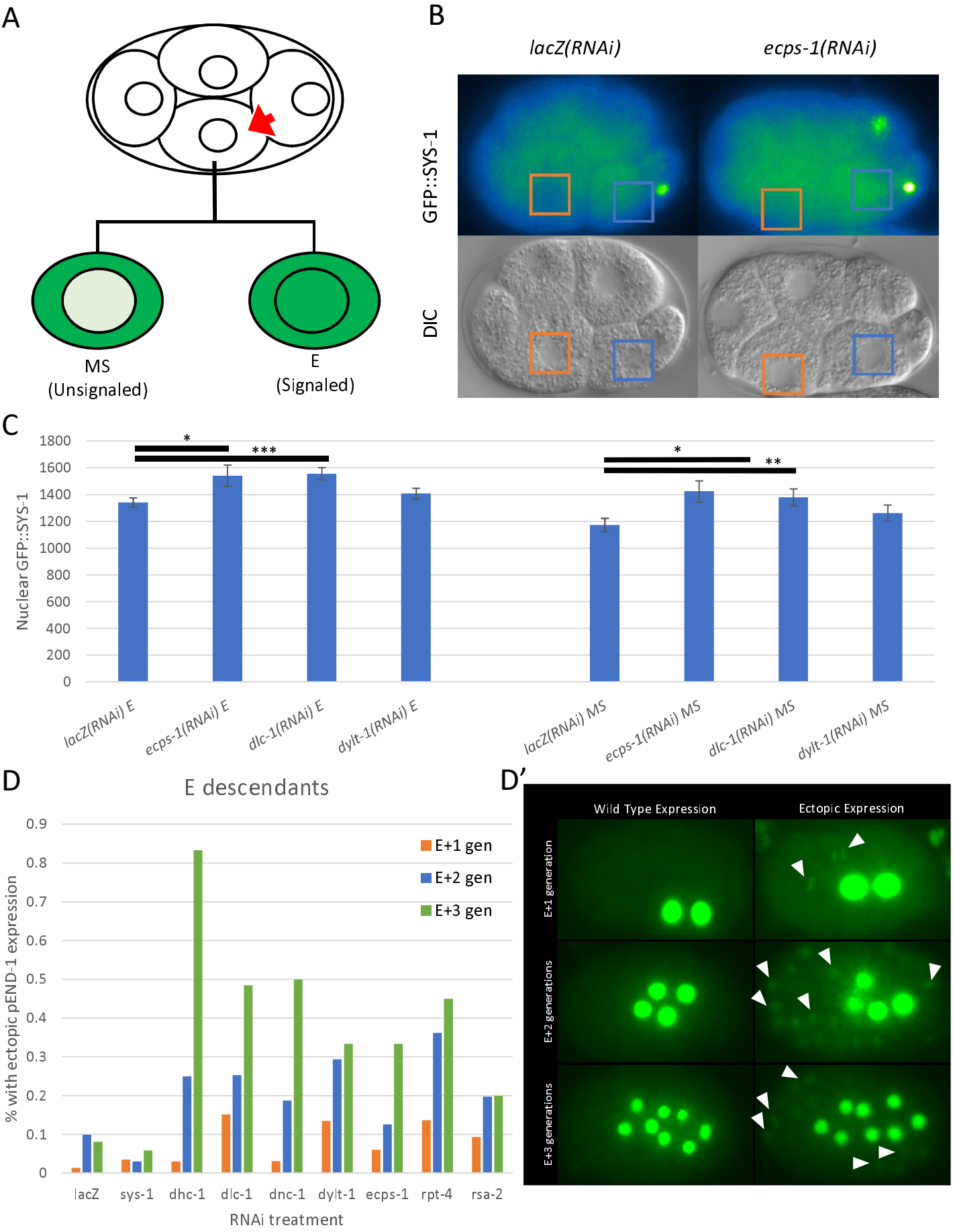
A
MS
(Unsignaled)
E
(Signaled)
B
lacZ(RNAi)
ecps-1(RNAi)
GFP::SYS-1
DIC
C
Nuclear GFP::SYS-1
1800
1600
1400
1200
1000
800
600
400
200
0
*
***
*
**
lacZ(RNAi) E
ecps-1(RNAi) E
dlc-1(RNAi) E
dylt-1(RNAi) E
lacZ(RNAi) MS
ecps-1(RNAi) MS
dlc-1(RNAi) MS
dylt-1(RNAi) MS
D
E descendants
% with ectopic pEND-1 expression
0.9
0.8
0.7
0.6
0.5
0.4
0.3
0.2
0.1
0
E+1 gen
E+2 gen
E+3 gen
lacZ
sys-1
dhc-1
dlc-1
dnc-1
dylt-1
ecps-1
rpt-4
rsa-2
RNAi treatment
D'
Wild Type Expression
Ectopic Expression
E+1 generation
E+2 generations
E+3 generations

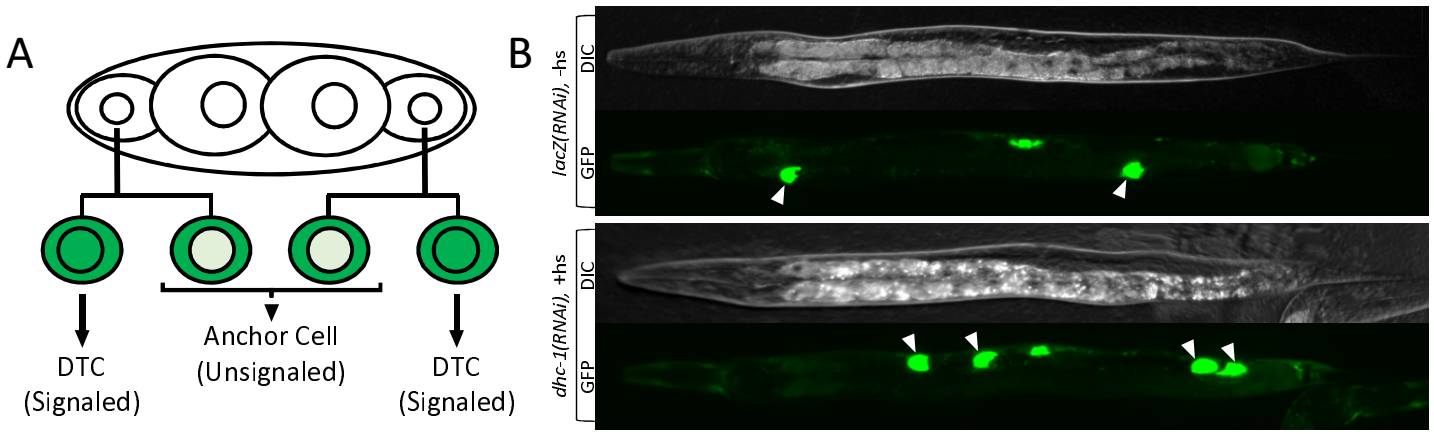

C

	0	1	2	3	4	5	6	
P_{hs}-sys-1 (no hs); lacZ(RNAi)		6.9%	93.1%					N=478
P_{hs}-sys-1 (no hs) sys-1(RNAi)	61.3%	32%	6.7%					N= 401
P_{hs}-sys-1(no hs) dhc-1(RNAi)		4.5%	95.2%	0.3%				N=310
P_{hs}-sys-1 (no hs) dlc-1(RNAi)		5.1%	94.9%					N=275
P_{hs}-sys-1 (no hs) dylt-1(RNAi)		7%	93%					N=172
P_{hs}-sys-1 (no hs) rsa-2(RNAi)		8.3%	91.3%	0.4%				N= 253
P_{hs}-sys-1 (no hs); ecps-1(RNAi)		7.6%	92.1%	0.3%				N= 394

Percentage of population
100%
80-99%
50-80%
30-50%
10-30%
5-10%
0.1-5%
0%

D

	0	1	2	3	4	5	6	
P_{hs}-sys-1(w/hs) lacZ(RNAi)		4.4%	69%	19.1%	5.4%	1.8%	0.3%	N=388
P_{hs}-sys-1(w/hs) sys-1(RNAi)	14.8%	30.7%	44.7%	7.8%	2%			N= 358
P_{hs}-sys-1(w/hs) dhc-1(RNAi) **		4.3%	58.1%	20.9%	15.5%	0.8%	0.4%	N=258
P_{hs}-sys-1(w/hs) dlc-1(RNAi)		4.2%	71.9%	18.2%	5.1%		0.6%	N=331
P_{hs}-sys-1(w/hs) dylt-1(RNAi) ***		6%	43%	33.3%	16.7%	0.5%	0.5%	N=186
P_{hs}-sys-1(w/hs) rsa-2(RNAi) *		4.4%	62%	23.5%	10.1%			N= 323
P_{hs}-sys-1(w/hs); ecps-1(RNAi) *		3.3%	64.4%	22.1%	8.3%	1.8%	0.3%	N= 399

A

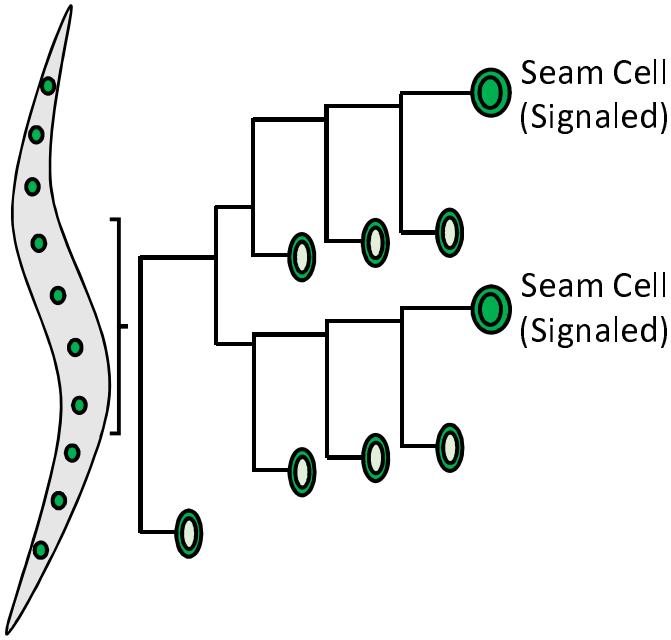

A'

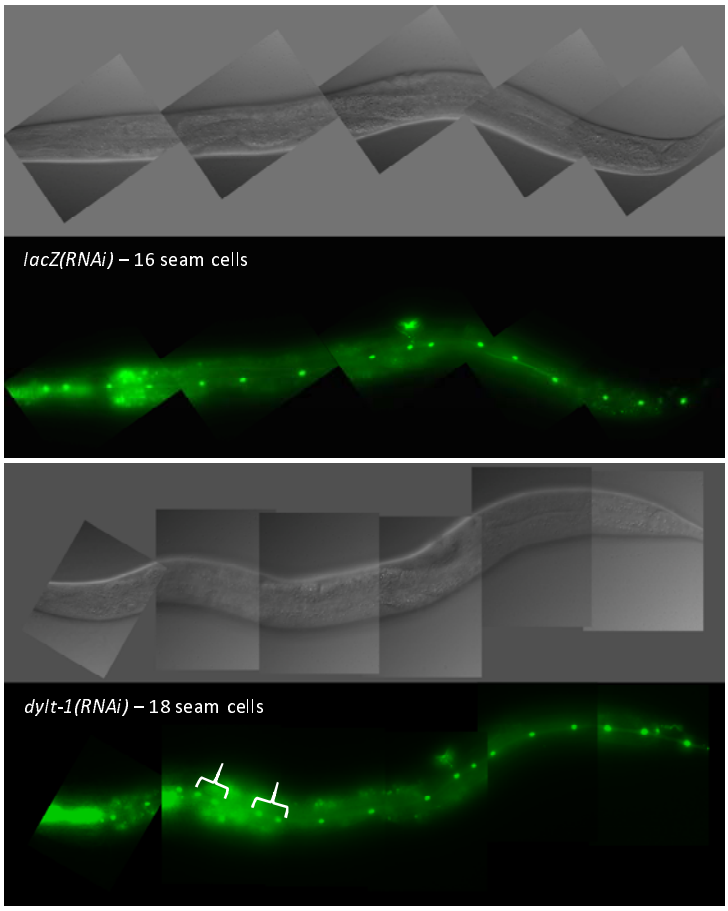

B

# of SCs	15	16	17	18	19	20	21	
P_{hs}-sys-1 (no hs); lacZ(RNAi)	1.7%	95%	3.3%					N=60
P_{hs}-sys-1 (no hs); dlc-1(RNAi) *		90%	8.3%			1.7%		N= 60
P_{hs}-sys-1 (no hs); dylt-1(RNAi) *		88.3%	10%			1.7%		N= 60

C

# of SCs	15	16	17	18	19	20	21	
P_{hs}-sys-1 (w/hs); lacZ(RNAi)	1.7%	80%	13.3%	5%				N=60
P_{hs}-sys-1 (w/hs); dlc-1(RNAi) **	1.7%	58.3%	33.3%	5%	1.7%			N= 60
P_{hs}-sys-1 (w/hs); dylt-1(RNAi) ***	1.7%	38.2%	26.7%	11.7%	11.7%	5%	5%	N= 60

Percentage of population

- 100%
- 80-99%
- 50-80%
- 30-50%
- 10-30%
- 5-10%
- 0.1-5%
- 0%

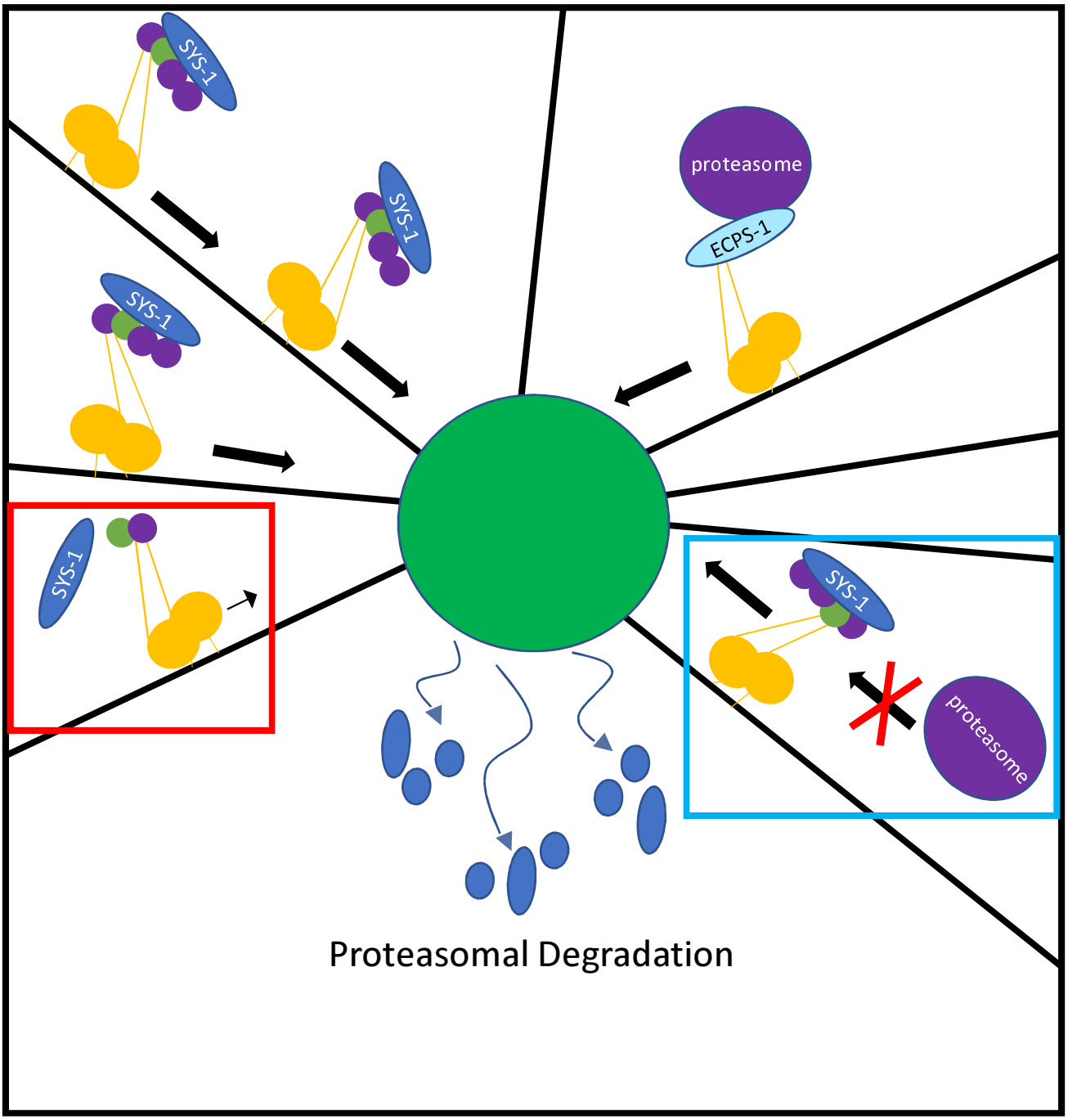
SYS-1
SYS-1
SYS-1
proteasome
ECPS-1
SYS-1
SYS-1
proteasome
Proteasomal Degradation